Bull Volcanol (2013) 75:714
DOI 10.1007/s00445-013-0714-5

RESEARCH ARTICLE

Impact of volcanism on the evolution of Lake Van I: evolution of explosive volcanism of Nemrut Volcano (eastern Anatolia) during the past >400,000 years

Mari Sumita · Hans-Ulrich Schmincke

Received: 20 February 2013 / Accepted: 19 March 2013 / Published online: 27 April 2013

Abstract The historically active Nemrut Volcano (2,948 m asl) (Eastern Anatolia), rising close to the western shore of huge alkaline Lake Van, has been the source of intense Plinian eruptions for >530,000 years (drilled lake sediments). About 40 widespread, newly recognized trachytic and less common rhyolitic fallout tephras and ca. 12 interbedded ignimbrites, sourced in Nemrut Volcano, are documented in stratigraphic traverses throughout an area of >6,000 km^2 mostly west of Lake Van. Phenocrysts in the moderately peralkaline trachytes and rarer large-volume comenditic rhyolites comprise anorthoclase, hedenbergite-augite, fayalite and, especially in trachytic units, augite, minor aenigmatite, apatite and quartz, and rare chevkinite and zircon. Dacitic to rhyolitic tephras from nearby calcalkalic Süphan Volcano (4,058 m asl), locally interbedded with Nemrut tephras, are characterized by disequilibrium phenocryst assemblages (biotite, augitic clinopyroxene and hypersthene, minor olivine, common crystal clots and/or, in some deposits, amphibole). The magma volume (DRE) of the largest Nemrut tephra sheet (AP-1) described in detail may exceed 30 km^3. Extreme facies and systematic compositional changes are documented in the ca. 30 ka Nemrut Formation (NF) deposits formed from one large and complex eruption (thick rhyolitic fallout overlain by ignimbrite, welded agglutinate, overbank surge deposits, and final more mafic fallout deposits). Common evidence of magma mixing in Nemrut ignimbrites reflects eruption from compositionally zoned magma reservoirs. Several young Çekmece Formation trachytes overlying ca. 30 ka old NF deposits and the late trachytes of the NF deposits show compositional affinities to tephra from Süphan Volcano possibly due to temporary influx of Süphan magmas into the Nemrut system following the evacuation of >10 km^3 magma (DRE) during the caldera-forming NF eruption. Axes of large fallout fans are dominantly SW–NE but W–E in the younger sheets resembling the direction of the present dominant wind field. Growth of Nemrut volcanic edifice and its peripheral domes since before 0.5 Ma in the hinge area between the Van and Muş tectonic basins is likely to have been the major factor in isolating Lake Van basin thus initiating the origin and subsequent alkaline evolution of the lake. This alkalinity was later significantly controlled by climate forcing. Internal forcing mechanisms (volcanic and geodynamic) may also have contributed to major lake level changes in addition to climate forcing.

Keywords Nemrut Volcano · Lake Van · Süphan Volcano · Tephrostratigraphy · Intraplate peralkaline trachytes and rhyolites · Agglutinate · PaleoVan

Introduction and goals

Huge alkaline Lake Van (130 km WSW–ENE extent, maximum depth 450 m, area ca. 3,755 km^2, present lake level at 1,648 m asl) in Eastern Anatolia is bordered by two large volcanic edifices: Nemrut Volcano (2,948 m asl), the most active volcano of Turkey having erupted basaltic and rhyolitic lava historically, is best known for its impressive caldera (Fig. 1). The volcano has grown between the tectonic and morphological pull-apart basins of Van Basin to the east and the Muş Graben to the southwest and is of alkaline intraplate character. Towering subalkaline Süphan Volcano

Editorial responsibility: J.D.L. White

M. Sumita (✉) · H.-U. Schmincke
GEOMAR Helmholtz Centre for Ocean Research Kiel,
Wischhofstr. 1,
24148, Kiel, Germany
e-mail: msumita@geomar.de

H.-U. Schmincke
e-mail: h-u.schmincke@t-online.de

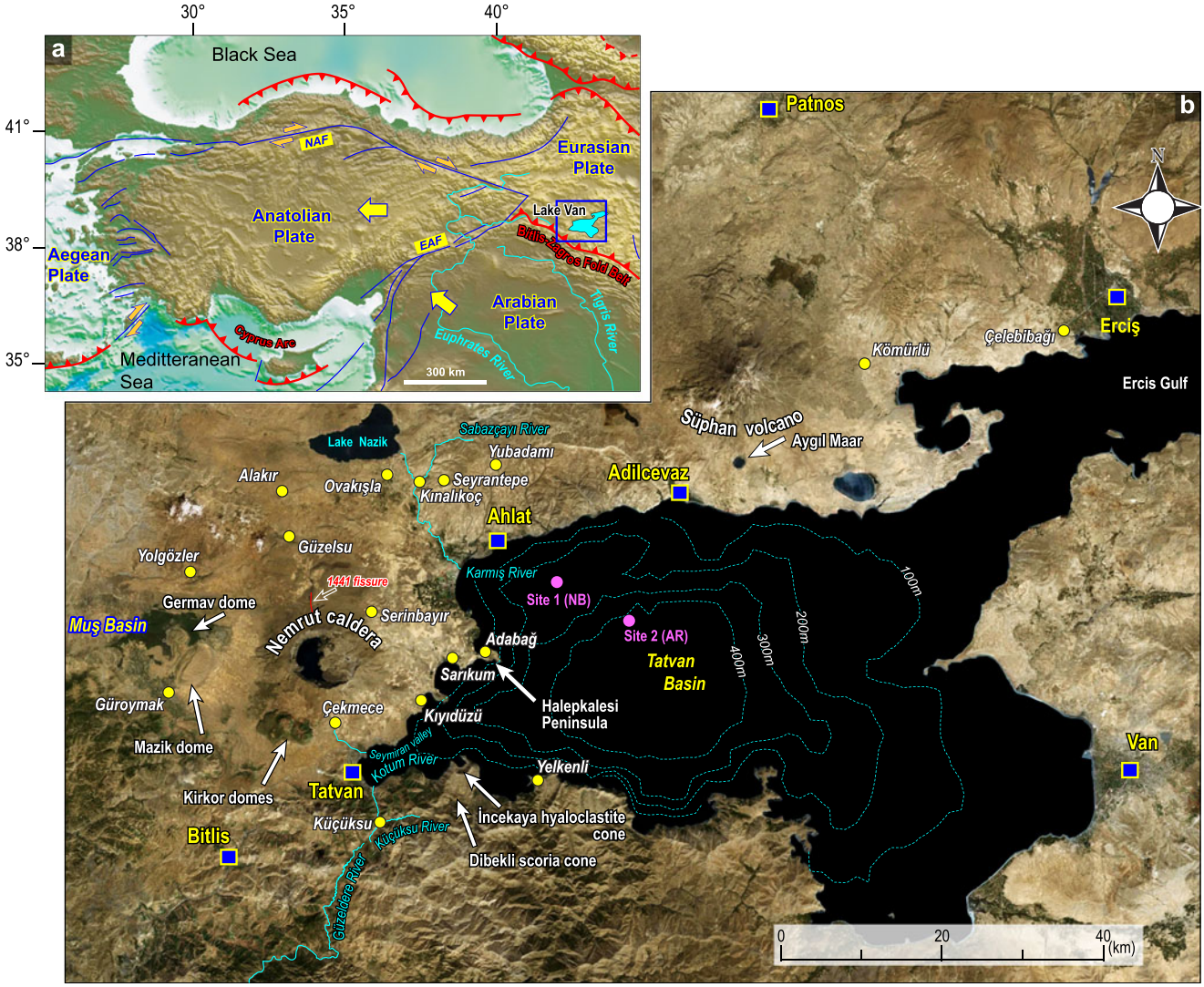

Fig. 1 **a** Anatolian, Eurasian, and Arabian plates with Lake Van just north of the collision zone (Bitlis-Zagros Fault Belt). Tectonic elements partly after Taymaz et al. (2007). **b** Map of Lake Van, volcanic edifices Nemrut and Süphan, major localities mentioned in the text and PaleoVan drill sites 1 and 2. Base map adapted from Google Earth (2012) Cnes/Spot Image

(4,058 m asl) rises ca. 60 km northeast of Nemrut. The large volcanic edifices are fed by highly contrasting magma sources, illustrating the complexity of the collision zone between the Arabian and Eurasian plates.

The most recent manifestation of ongoing tectonic and seismic activity in the Lake Van area was the devastating *M*7.2 Van–Erciş earthquake on October 23, 2011. The effect of lithospheric loading on earthquake triggering even by minor Van lake level changes has been demonstrated, with temporal correlations of seismicity with the water level changes "very persuasive and dramatic, indicating hydrogeological triggering of the earthquakes" (Utkucu 2006). Many young dominantly east–west, north–south and northeast–southwest-aligned faults extend across the area (Horason and Boztepe-Güney 2007; Selcuk et al. 2010) and cut the pyroclastic cover (see below). The Van lake basin is subdivided tectonically into several grabens and half grabens and has been shortened by ca. 2 km during its evolution (Cukur et al. 2012). East–west and northeast-trending tectonic structures dominate the basin floor.

Tephra from both volcanoes has contributed significantly to the sediment fill and probably to the alkaline composition of the lake. The alkaline composition of Lake Van and the drastic oscillations of lake level (volume) are traditionally thought to have been governed dominantly—if not exclusively—by climate (e.g., Degens and Kurtmann 1978; Kuzucuoğlu et al. 2010 and literature therein), the age of the lake basin's isolation being placed most recently at ca. 100–130 ka (Kuzucuoğlu et al. 2010).

Our study of the products of explosive eruptions, chiefly in the eastern and northern slopes of Nemrut Volcano, began in 2008 as a pre-site survey for the ICDP PaleoVan drilling project (Litt et al. 2011). That project has the goal of

reconstructing the compositional evolution of the lake, using tephra deposits to establish its chronology within the tectonically and volcanically highly active closed Lake Van Basin, and to then reconstruct the basin's climatic and geodynamic evolution. We here focus on the overall stratigraphy and compositional characteristics of widespread Plinian fallout deposits and ignimbrites, dominantly from Nemrut Volcano, throughout a large area between the towns of Van–Bitlis–Muş–Tatvan–Ahlat and Erciş in order to provide a rigorous stratigraphic, compositional and temporal framework for the PaleoVan drilling project. We also assess the timing and cause of the isolation of the lake, its alkaline character and the total mass of volcanic materials transferred into the lake over time. The scant published information of pyroclastic deposits in the area necessitates a basic documentation, especially since the tephra deposits found by us are spread over a large region in overwhelming abundance. We discuss two representative fallout and flow eruptive units in more detail in order to illustrate the volcanological and compositional complexities of large-volume tephra deposits from Nemrut Volcano. We also briefly characterize Süphan tephras that are interbedded with those from Nemrut, such knowledge being indispensable to reconstruct the evolution of the Nemrut system. We briefly discuss climate impact, environmental proxies and volcanic hazards. The major goal of our work and that of this paper is to document and understand the relative roles in time and space of the major forcing factors—tectonic, volcanic and climatic—of the Nemrut–Lake Van geosystem since its initiation more than 0.5 million years ago.

Geological setting

The origin of the East Anatolian plateau is generally explained by collision of the Arabian Peninsula with the Eurasian plate leading to uplift of an area of >20,000 km^2. The overall geodynamic setting and the evolution of collision, uplift, and subsequent volcanism since the Middle Miocene is discussed in Dewey et al. (1986); Pearce et al. (1990); Şengör et al. (2003); Keskin (2003, 2007) and literature therein. The area coincides with the extent of the Eastern Anatolian Accretionary Complex. Slab-steepening and breakoff is invoked to explain voluminous magma generation in the Middle Miocene. The mantle lithosphere is either very thin or absent beneath a considerable portion of the region, and collision, uplift and magma generation at depth are closely connected. Post-collisional volcanism in the area started at about 8–6 Ma (though possibly as early as 16 Ma according to our data from the PaleoVan drilling (Litt et al. 2012)), with the younger age following the start of major uplift at about 12 Ma (Pearce et al. 1990). As a result of the collision, the North Anatolian block bound in the south by the left-lateral East Anatolian fault, and in the north by the right-lateral strike-slip North Anatolian fault moved westwards, with the Muş and adjacent Van basins being formed as pull-apart basins chiefly from strike-slip motion of the North Anatolian fault. Pearce et al. (1990) present a broad account of volcanism in eastern Turkey with a focus on the nature of magma sources based on chemical compositions and isotope ratios of selected volcanic rocks.

Previous work

Deposits of *explosive* eruptions of Nemrut and Süphan volcanoes have previously received only passing attention. Yılmaz et al. (1998) postulated 5 evolutionary phases for Nemrut—as for the other East Anatolian volcanoes: pre-construction, cone building, climactic, post-caldera, and late phase. Aydar et al. (2003) distinguish a construction and destruction phase of what they call pre- and post-caldera stage. They consider fissure-fed basalts and scoria cones, dated by Pearce et al. (1990) as 1.18±0.23 Ma, as the oldest products of the construction phase. As discussed by Sumita and Schmincke (2013a) this age was determined on historic lavas erupted in 1441 AD, the age being attributed to excess argon by Pearce et al. (1990). The idea of Nemrut volcanism having begun ca. 1 million years ago is still maintained (e.g., Ulusoy et al. 2012) but *published* evidence is lacking. Aydar et al. (2003) envision an early destruction phase to have produced thick Plinian fall and ignimbrites with a postulated volume of 40 km^3 spread over an area of 86 km^2, followed by caldera collapse. This collapse is thought by most earlier authors to have occurred ca. 0.30 million years ago, the age of eccentrically located trachytic Kirkor dome on the east flank of Nemrut cone (Ercan et al. (1990) quoted in Aydar et al. (2003)). Karaoğlu et al. (2005) basically imply that the caldera formed following eruption of what is frequently called "Nemrut Ignimbrite". This ignimbrite is, however, a relatively young product of the explosive activity of Nemrut Volcano dated by us as ca. 30 ka; unfortunately, several different ignimbrites have been called "Nemrut Ignimbrite" in the literature as discussed below.

Aydar et al. (2003) consider basalts and trachytes to be the dominant rock type of the young flank eruptions of Nemrut. They mention two pre-caldera ignimbrites, the younger of which, called Nemrut Ignimbrite and interpreted to be associated with the development of Nemrut Caldera, is the main subject of the study by Karaoğlu et al. (2005). Özdemir et al. (2006), like Karaoğlu et al. (2005), distinguish three major evolutionary stages, their pre-caldera stage being further subdivided into effusive, extrusive and explosive phases, the latter being responsible for caldera formation. They present a geological map of the Nemrut

Volcano area and 30 major and trace-element analyses of lava flows and domes. They also postulate pyroclastic pre-caldera deposits to have been deposited in three phases, subdivided by paleosols and estimate that eruption of 62.6 km^3 pyroclastic material was responsible for caldera collapse. Çubukçu et al. (2012) studied Nemrut lavas petrologically. Ulusoy et al. (2012) subdivide the evolution of Nemrut Volcano into a pre-caldera (1 Ma–80 ka) period, which they subdivide into 3 stages. (I: 1 Ma–300 ka; II: 300 ka–200 ka; and III: 200 ka–80ka) followed by a syn-caldera stage (80–30 ka). They postulate that the caldera collapse was associated with the eruption of two fallout-ignimbrite associations: an older very widespread Nemrut Ignimbrite and an overlying Kantaşi Ignimbrite. Ulusoy et al. (2012), like Çubukçu et al. (2012), assume that the present Nemrut Caldera collapsed sometime between 90 and 30 ka with their Nemrut and Kantaşi stratigraphic units consequently having erupted during this time interval. We will discuss their detailed correlations below. Sumita and Schmincke (2013a) postulated several caldera stages based on 32 single crystal $^{40}Ar/^{39}Ar$ ages and bulk chemical analyses of fallout tephra and ignimbrites. Holocene lava flows and domes and some phreatomagmatic deposits form the youngest fill of the caldera, some 10 km^2 of which is occupied by a lake up to 150 m deep.

Tephra layers recovered in shallow cores in Lake Van (e.g., Landmann et al. 1996; Litt et al. 2009) range in *varve age* from ca 510 AD to 13,585 BP. İncekaya, Süphan, and Nemrut are thought to be potential centers for these young tephra layers (Ulusoy et al. 2008). İncekaya hyaloclastite cone (Fig. 1) erupted ca 80,000 years ago as shown by its land stratigraphy (Sumita and Schmincke 2013a) and can be considered extinct. All Holocene tephras are related to Nemrut while five late-glacial tephras near the base of these short cores were sourced in Süphan based on their glass and mineral composition (Sumita and Schmincke 2009). In 1441 AD, several basalt lavas and a subsequent rhyolite obsidian flow erupted from a north–south-oriented fissure close to the northern caldera rim (Karakhanian et al. 2002). The descriptions of a subaqueous eruption in Lake Van on October 27, 1650 (Haroutiunian 2006) resemble those of shallow submarine eruptions such as that of El Hierro in 2011–2012 and others in remarkable detail (Schmincke and Sumita 2013). The question whether one of these two historic eruptions—or neither—is related to the youngest tephra layer recovered in the short cores is under study together with analysis of ca. 300 tephra layers drilled in the PaleoVan ICDP Project in several holes at two sites, one 220 m deep, in Lake Van in 2010 (Litt et al. 2011, 2012).

Methods

Our reconnaissance fieldwork was carried out dominantly around the western part of Lake Van (Figs. 1, 2). We have focused on pyroclastic deposits to provide a basic stratigraphic, lithological–compositional, and temporal framework for the ICDP-drilling project (PaleoVan). Field correlation based on characteristic aspects of tephra layers (grain size, grading, thickness, color, special structures, phenocrysts, marker horizons, stratigraphic position etc.) was aided by distinct marker horizons, phenocryst, glass, and whole rock compositions (see below) and single crystal $^{40}Ar/^{39}Ar$ ages. Methods for XRF and EMP analyses are listed in the Appendix, those for single crystal dating and additional whole rock analyses are shown in Sumita and Schmincke (2013a, b).

We have used classic stratigraphic nomenclature: *Member* for distinct mappable units such as individual fallout tephra or ignimbrite units, *Formation* for several members representing a larger stratigraphic unit while *Group* includes several formations. Locality numbers are shown in Sumita and Schmincke (2013a: Fig. 3 and the supplement).

Regional tephrostratigraphy

Characteristic tephra units were stratigraphically correlated over some 6,000 km^2, here presented in composite stratigraphic sections from 4 major areas, including mineralogical and chemical characteristics and ages where available for each of the three major traverses (Fig. 2; see also Fig. 4 in Sumita and Schmincke (2013a)).

We call buff, dominantly fine-grained, moderately to poorly sorted, structurally highly varied intervals of amalgamated massive to bedded reworked tephra and discontinuous remnants of centimeter- to decimeter-thick primary fall layers and/or unwelded ignimbrites *Inter-Tephra Deposits* (*ITD*) (Fig. 2). Their thickness varies from a few centimeters to >2 m. In the well-dated main Ahlat section (Fig. 3), many of these intervals represent some 20 to 50 ky that separated major explosive events. They can, of course, locally represent much shorter intervals depending on the contrasting climate impact north and south of Lake Van and thus degree of erosion during a particular climate stage, etc. Most of the local remnants of one or more fall and ignimbrite deposits within the ITDs could represent eruptions of smaller magnitude or were severely removed during periods of more intense erosion. We estimate that volcanic material makes up >90 % of most ITDs. This is important when assessing the mass of primary and secondary volcanic materials supplied to Lake Van over time. Overprinting by soil-forming processes is less pronounced in the morphologically subdued areas north and west—compared to the precipitous mountains south of Lake Van—reflecting dry climate through the time interval considered.

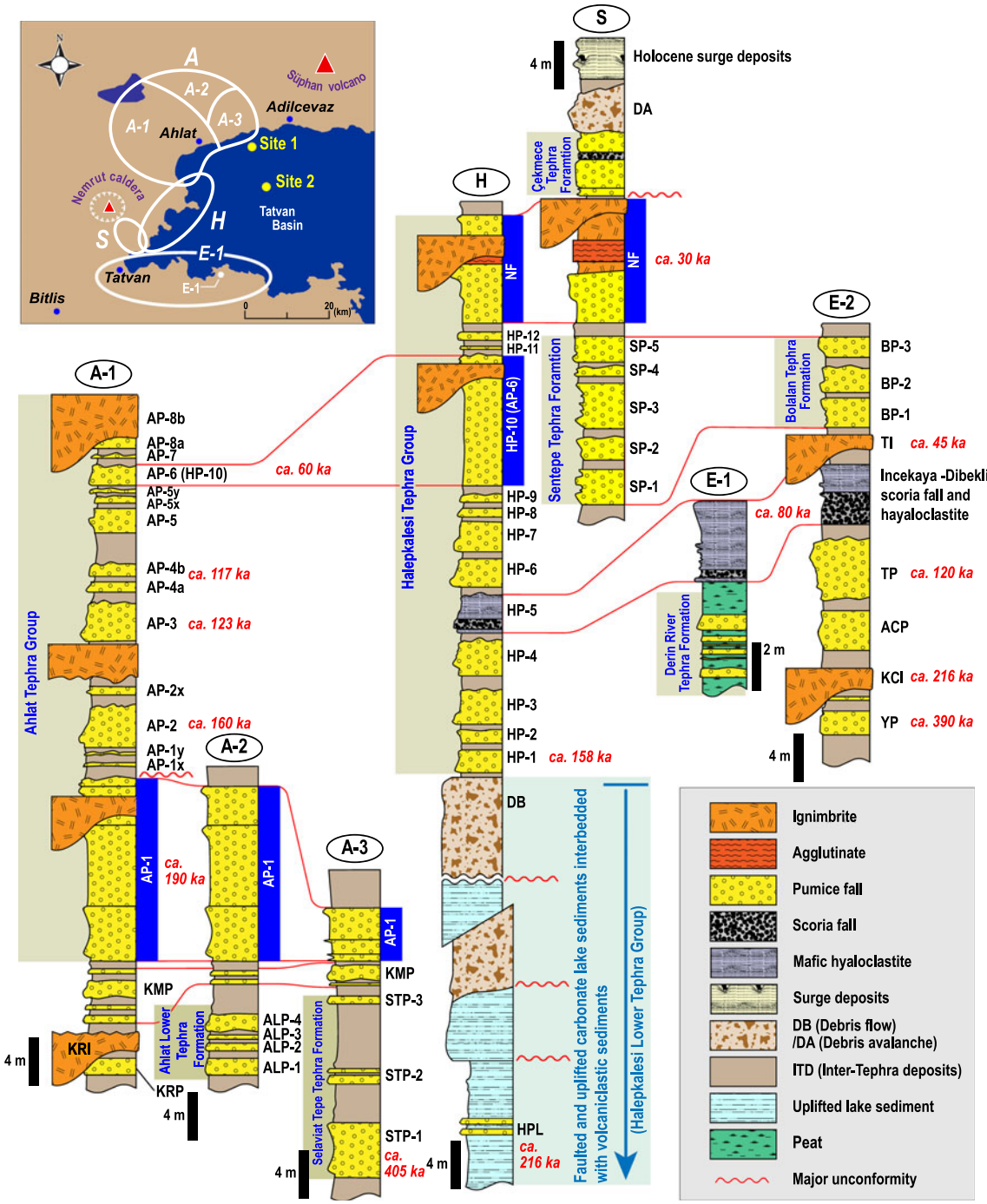

Fig. 2 Composite stratigraphic sections of Nemrut tephra deposits in four major areas. *A* Ahlat area (*A-1* southwestern Lake Nazik-town of Ahlat; *A-2* north of Ahlat; *A-3* east of Ahlat). *H* western coast area between Halepkalesi Peninsula and northeast of Tatvan. *S* Şentepe area at southeastern slope of Nemrut. *E* eastern Tatvan area (*E-1* tephra layers exposed in swamp deposit south of Yelkenli; *E-2* composite sections of eastern Tatvan area). Abbreviations (for details see also Sumita and Schmincke (2013a)): *ACP* Alacabük Pumice; *AP* Ahlat Pumice; *ALP* Ahlat Lower Pumice; *BP* Bolalan Pumice; *DA* debris avalanche; *DB* debris flow; *HP* Halepkalesi Pumice; *HPL* Halepkalesi Lower Pumice; *KCI* Küçüksu Ignimbrite; *KMP* Karmiş Pumice; *KRI* Karak River Ignimbrite; *KRP* Karak River Pumice; *NF* Nemrut Formation; *SP* Şentepe Pumice; *STP* Selaviat Tepe Pumice; *TI* Tatvan Ignimbrite; *TP* Tatvan Pumice; *YP* Yelkenli Pumice

Stratigraphy of Plinian fall deposits

A couple of distinct Plinian pumice lapilli fall deposits were recognized around Lake Van (Karaoğlu et al. 2005) but their stratigraphy, thickness variation, volcanological parameters, lateral extent (and thus magnitude of the eruptions), composition, age and orientation of depositional fan axes were unknown. We will discuss the recent stratigraphic

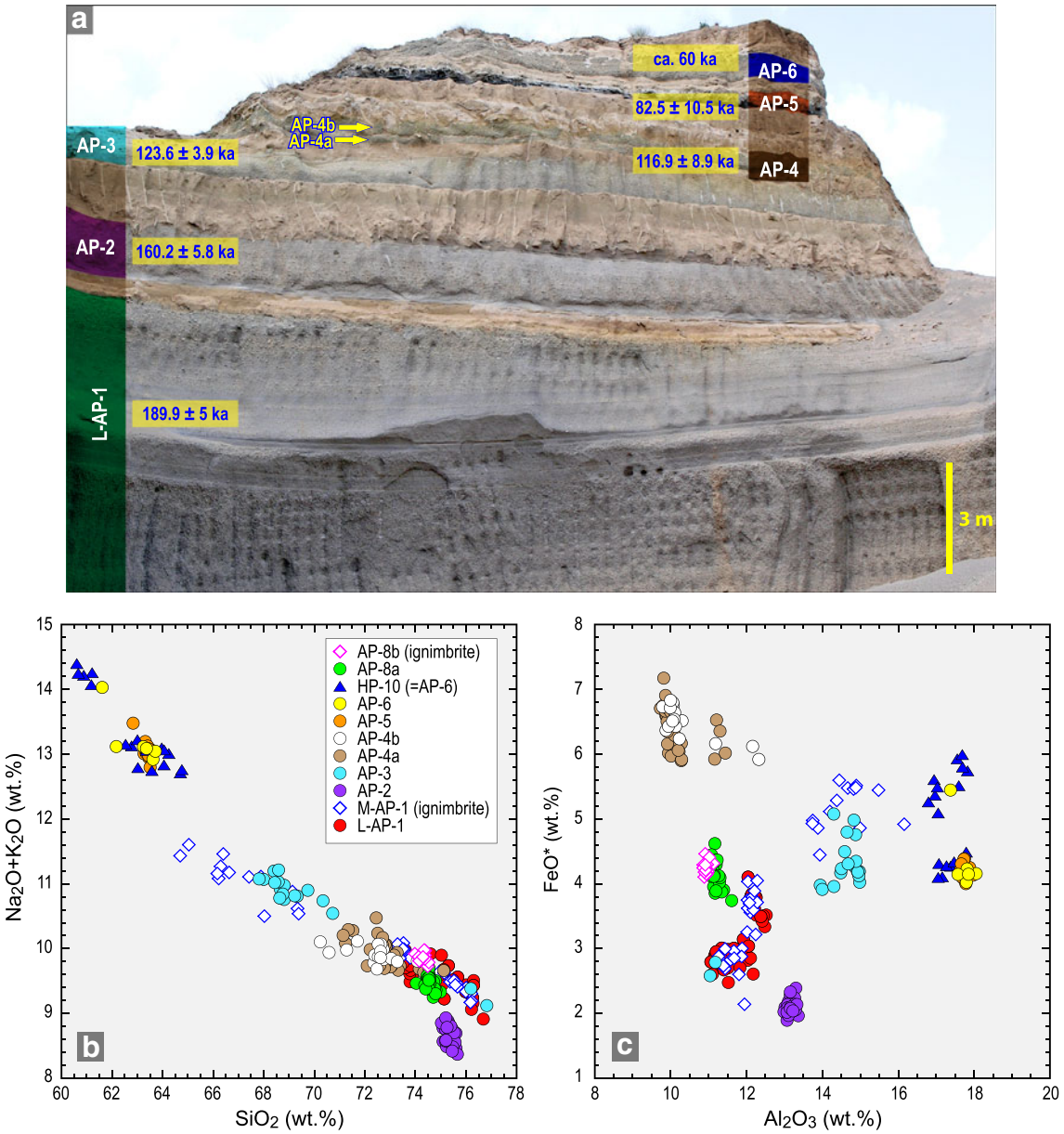

Fig. 3 **a** Stratigraphic section 5 km west of Ahlat (loc. 25) showing major units AP-1 to AP-8 with ages. Age data from Sumita and Schmincke (2013a). **b** SiO_2 vs. total alkalis; **c** FeO* vs. Al_2O_3 to highlight peralkaline compositions (both EMP analyses of glass shards). Variation diagrams also include tephra units not shown in Fig. 5a (e.g., AP-8a, AP-8b, HP-10, M-AP-1)

correlations of Ulusoy et al. (2012) following our general stratigraphic descriptions.

So far, we have discovered—and correlated some over tens of kilometers—at least six *large-volume* dominantly rhyolitic pumice fallout deposits (on-land thickness >5 m at 5 km distance from Nemrut Caldera), and >30 medium-scale mostly trachytic fallout deposits erupted over the past ca. 400 ky (Fig. 2). The large-magnitude explosive eruptions are documented by (1) thickness—practically all eroded at the top—at some 25 km distance from Nemrut Caldera, the presumed source; (2) the diameter of pumice bombs (up to 50 cm (!) in some) and (3) the minimum magma volumes (DRE). One fallout unit (Ahlat Pumice-1: AP-1; Fig. 3; described in more detail below), up to ca. 15 m (!) thick near Ahlat 25 km away from the source (calculated magma volume >30 km^3 DRE), would have completely buried the town except for the top of the highest minaret towers if it had happened recently (e.g., Fig. 5). Outcrops (data density) are insufficient to calculate a more precise DRE volume. Nevertheless, magma volumes of the large sheets (up to tens of cubic kilometers) are in the range of some of the larger Plinian eruptions known (Fisher and Schmincke 1984).

Most pumice fall sheets are composed of several subunits following each other in a systematic pattern. (1) A basal layer of fine- to medium-grained well-sorted coarse ash to fine lapilli, generally <10 cm thick, underlies many large tephra sheets with a sharp upper boundary (e.g., Fig. 6b). (2) The bulk of the lower and often main part of a tephra sheet is generally unbedded (in some units consisting of several units), and separated from overlying subunits by thin layers rich in hydrothermally altered lithics. (3) A middle subunit is commonly layered, slightly finer-grained, slightly less well sorted and with some showing inverse grading and others consisting of several thinner subunits (e.g., Fig. 6a). (4) The top subunit in many fall sheets is massive to chaotic and coarse-grained but always variably eroded. An ash fraction is generally absent at medial distances (ca. 15–30 km from vent), except in layers a few centimeters thick at the base or in the central subunit of a fall unit. Phenocrysts are commonly sparse (≪5 vol.%) in the lower subunit(s)—except in the fine-grained basal ash layer of some sheets—but may increase to <5 vol.% in the upper subunits. Fresh lithics, generally <3 vol.%, comprise obsidian and, in some units, basalt clasts some clearly mixed with rhyolitic pumice, suggesting magma mingling and injection of basaltic magma into the resident evolved magma body.

Fallout sheets older than ca. 60 ka have not been found in the mostly shallow ravines along the proximal slopes of Nemrut edifice. More thorough dissection of tephra packages in the mountain valleys east of Tatvan and north of Ahlat, however, has exposed tephras as old as 400 ka (Sumita and Schmincke 2013a). Erosion has generally been much more severe in the Bitlis massif mountains south of Lake Van, marked by wetter climate and thus more intense weathering.

Our stratigraphy is at variance with the stratigraphic correlations of Ulusoy et al. (2012).

1. More or less abrupt grain size changes in fallout sheets interpreted by Ulusoy et al. (2012) as distinct fallout events (examples: XF2 and XF3 in their Fig. 3b and c, and NeF1 and NeF2 in their Fig. 3d) are interpreted by us as subunits of specific fallout members subdivided as described above, reflecting collapse and re-establishment of eruption columns and changes in mass output rate, not stratigraphically distinct fall units. Such subunits can laterally merge and drastically change in grain size and thickness.
2. Our evidence is incompatible with the correlation of all major units proposed by Ulusoy et al. (2012). For example, XF4 (their Fig. 3c) is actually identical to NeF1 and NeF2 (both are only subunits) in their Fig. 3b and d. Units XF2 and XF3 (their Fig. 3c) on the other hand, correspond to our trachytic HP-10 (Fig. 2, this paper), and are identical to their XF4 in their Fig. 3d. Their NeF1 is the finer-grained base of NeF2—both are equivalent to the rhyolitic fallout, the lowest member (L-NF) of the Nemrut Formation (NF) as discussed in detail below.
3. We disagree with the identification of some units as reworked (Rw) by Ulusoy et al. (2012). For example, Rw in their Fig. 3c is not reworked material but the coarse-grained upper part of L-NF. The Rw overlying their XF3 in Fig. 3b is the ignimbrite overbank deposit, locally surge-like, of NF and does not represent a period of reworking (see, e.g., Fig. 9b in Sumita and Schmincke (2013a)).
4. We disagree with the regional tephra correlations of Ulusoy et al. (2012). For example, at their locality 58, ca. 1 km west of Ahlat (their Fig. 5), they correlate the lower part of the section (their unit XF2, XF3 and XF4) to the southern section well exposed in two large quarries west and southwest of Sarıkum (their localities 14 and 15). In our view, however, the lower part of the section at their locality 58 begins with AP-1, a huge rhyolitic fallout unit dated as ca. 190 ka (Sumita and Schmincke 2013a), overlain by rhyolitic AP-2 (ca. 170 ka), trachytic AP-3 (ca. 140 ka), etc., as also shown in Fig. 3 in this paper, while their tephra unit called XF2 and XF3 at the southern localities in their Fig. 3c is equivalent to our HP-10 (ca. 60 ka). XF2 in their Fig. 3b is equivalent to our L-NF dated at ca. 30 ka (Sumita and Schmincke 2013a).

   Our tephrostratigraphy is based foremost on field criteria but all major units have also been characterized by their qualitative and quantitative mineralogy, rock and/or glass composition and $^{40}Ar/^{39}Ar$ single crystal ages. The high-precision stratigraphy that we attempt is indispensable for allowing convincing correlations with at least some major units of the ca. 300 mostly thin tephra layers drilled in Lake Van.

Stratigraphy of ignimbrites

Previous work

About two to three ignimbrites on and around Nemrut Volcano have been mentioned previously in the literature: the Nemrut Ignimbrite, so far not studied in detail, dated at ca. 30 ka (our dates in Sumita and Schmincke (2013a)), and an “older” Bitlis Ignimbrite at the town of Bitlis extending for at least 40 km south of Nemrut (e.g., Karaoğlu et al. 2005; Özdemir et al. 2006) that some authors (e.g., Ulusoy et al. 2012) correlate with the Nemrut Ignimbrite. Mouralis et al. (2010) and Kuzucuoğlu et al. (2010) in their study of Lake Van terraces mention three ignimbrites: (a) Bitlis flow north of Tatvan, also equated with Nemrut Ignimbrite, is

correlated to a black ignimbrite cropping out along Küçüksu River—called "Obuz Ignimbrite" or "BPF" (Black Pumice Flow) by these authors and to the Nemrut Ignimbrite of Çubukçu et al. (2007) based on its trachytic composition. (b) A younger ignimbrite, called "Kotum Ignimbrite", is believed to begin as a relatively small tongue at the southern rim of Nemrut Caldera that extended into Kotum and Güzeldere River canyons south of Tatvan. Our correlations, age relationships and interpretations do not agree with the interpretations in the literature as discussed below. "NeIg" of Ulusoy et al. (2012), called Nemrut Ignimbrite in their Fig. 7, is identical to their KaIg2 (their Kantaşi Ignimbrite). We think the Nemrut and Kantaşi units represent a single, albeit complex, depositional unit. Ulusoy et al. (2012) interpret the ignimbrite as consisting of one flow but we found Nemrut Ignimbrite to consist of at least three flow units as in the valley-filling Nemrut Ignimbrite at the village of Çekmece. This is significant because, interestingly, the agglutinate facies of the Nemrut Formation (NF) (described below) also seems to consist of three subunits, which we tentatively correlate with the flow units of the valley facies.

Stratigraphy in the western–southern area (Muş–Halepkalesi–Tatvan area)

We have recognized more than ten ignimbrites all probably sourced in Nemrut and have dated eight of them directly or indirectly by their underlying cogenetic fallout tephra (Sumita and Schmincke 2013a). The oldest ignimbrite dated so far by us has an age of 264.10±2.75 ka. This Muş Ignimbrite (MUI) covers the uplifted graben shoulder north of the Muş Graben and underlies the ca. 190 ka tephra AP-1 fall deposit and ignimbrite.

Correlation of ignimbrites in the area is difficult due to strong contrasts between valley and overbank facies and pronounced compositional zoning. Older ignimbrites are not well exposed except locally, as along cliffs of Savazçayı River (east of Lake Nazik), and are thus difficult to correlate stratigraphically because they share similar major mineralogical and chemical characteristics. All of the older ignimbrites recognized are represented by plateau facies only. Complex surge deposits are common at the base of some ignimbrites, especially below the young Nemrut Ignimbrite (e.g., Fig. 9).

The Tatvan Ignimbrite (TI) (ca. 45 ka) (type locality along the road Tatvan–Van (route D-300) just outside Tatvan where it overlies İncekaya hyaloclastite and Tatvan Pumice (TP) (Fig. 8f in Sumita and Schmincke (2013a)) may have advanced across Lake Van for at least several kilometers, because 10–20-m-thick primary TI deposits are found on the opposite side of the lake east of Tatvan close to İncekaya hyaloclastite cone (Fig. 1). Alternatively, the flow was erupted during a major low stand of the lake level, and we present strong evidence below that prior to ca. 30 ka lake level was indeed much lower than at present. An ignimbrite exposed near Dalda in a mountain valley south of Tatvan (Ulusoy et al. 2012) may be correlative with TI. At least one other pyroclastic flow (the prominent black *Küçüksu Ignimbrite*: KCI) must have overtopped a 2,600 m high mountain (the town of Tatvan is at ca. 1,648 m asl) barrier between Nemrut Volcano and the canyon of Güzeldere River where the deposits exceed 10 m in thickness.

The TI (ca. 45 ka) is only slightly sintered in the bed of the Güzeldere River next to road D-300 and also shows locally weakly cemented degassing pipes. The basal KCI south of Tatvan was dated as ca. 216.4±14.3 ka (Sumita and Schmincke 2013a) even though its excellent preservation along *Küçüksu* River suggests a young age; KCI is significantly older than Nemrut Ignimbrite (our M-NF). Poorly defined Bitlis Ignimbrite—possibly more than one ignimbrite may exist in the Bitlis area—is probably also old (perhaps >200 ka). In the Ahlat–Lake Nazik area, we can recognize four or five ignimbrites, all significantly older than Nemrut Ignimbrite. Hydrothermally cemented and eroded degassing chimneys of the Nemrut Ignimbrite are spectacularly exposed near Tatvan (Fig. 9a in Sumita and Schmincke (2013a)).

In summary, we recognize ca. ten different ignimbrites although some may eventually be correlated between the Ahlat–Lake Nazik and the Tatvan areas. The youngest ignimbrites covering part or all of the huge flat Muş Graben may be correlative to M-NF. Some ignimbrites in the Tatvan area are valley-confined while superposition of probably at least three different large ignimbrite sheets has formed the extraordinarily flat surface of huge Muş Basin.

Stratigraphy of the northeastern area (Ahlat–Nazik)

The country between Ahlat and Lake Nazik is a subdued valley traversed by the Karmiş River, which debouches into Lake Van just south of Ahlat (Fig. 1). The gentle slope southwest of Karmiş River represents the northern slope of Nemrut while the country northeast of the river rises gradually for some 10 km, is faulted north and east of Ahlat and gently folded and faulted east of Lake Nazik. An unwelded ignimbrite underlying the famous Seldchuk cemetery on the southern outskirts of Ahlat extends in patches for several kilometers to the west where it locally represents the top deposit but is represented by a columnar intracanyon flow to the north along Savazçyı River (Fig. 7a in Sumita and Schmincke (2013a)). Several older ignimbrites occur in the deeper canyons to the north, especially north of the town of Ovakışla where the terrain forms a broad anticline cut by a central post-ignimbrite graben (see below). The source for the colorful building blocks of many older

houses in Ahlat is the more strongly welded part of an ignimbrite overlying AP-1.

Two case histories

Ahlat Pumice-1 (AP-1)

AP-1 is the most striking, and, owing to its tremendous thickness, stratigraphically and volumetrically most impressive tephra deposit in the entire pyroclastic Nemrut fan (Figs. 2, 3, 4, 5, and 6). The minimum thickness in several quarries around the town of Ahlat (Figs. 4, 5) is 12–15 m but the top is generally eroded. We assume an original thickness of >15 m for the Ahlat area, 21 km due NE of the center of Nemrut Caldera. The deposit consists of three major and several minor subunits.

Plinian fallout phase (L-AP-1: Lower Ahlat Pumice-1)

L-AP-1a AP-1 begins with a thin but ubiquitous basal ash layer generally <10 cm thick (Figs. 4, 6b), locally cross-bedded and crystal-enriched in some areas but crystal-free in others. This layer is interpreted to have been emplaced by fall, locally possibly also by surges. Similar fine-grained ash layers also occur at the base of AP-2 and TP. Wavy structures in this basal layer are commonly not due to lateral surge transport but to mantling of plants growing on the pre-eruption surface, but each locality has to be analyzed separately.

L-AP-1b The main massive basal unit is coarse-grained and well sorted, practically devoid of ash (Md ca. 1–1.5 cm at loc. 25). Its thickness decreases from 4 m (loc. 23) to 2.1 m (loc. 43) but MP (maximum pumice size) does not change much between these localities (loc. 23: 8 cm; loc. 27: 7 cm; loc. 43: 8 cm). This most monotonous unit (Fig. 6a, b) suggests unusually steady eruptive conditions during the first major phase of AP-1 eruption following vent enlargement. Several other Nemrut fall units show a similarly monotonous coarse-grained basal unit. The upper ca 50 cm of this unit is slightly coarser grained.

L-AP-1c to L-AP-1e This subunit, commonly 3–4 m thick in the pumice pits west of Ahlat, is distinctly layered on a gross scale, individual beds ranging from 0.8 to 1.5 m and differ from each other in grain size (Fig. 6a); an ash-size fraction is commonly lacking.

A coarser 10–20 cm interval of L-AP-1c and/or a distinct layer a few centimeters thick rich in dark volcanic (obsidian and/or basalt) and hydrothermally altered rock fragments overlies the basal unit commonly with a sharp boundary suggesting complete collapse of the eruption column. Mafic lapilli-sized domains also inside some white pumice lapilli and other textures reflect ubiquitous magma mingling.

L-AP-1f Grain size is at a maximum in the chaotic top unit of AP-1 as in several other sheets, tephra in some deposits being also more poorly sorted (an ash fraction, however, is generally lacking). Scattered larger decimeter-sized pumice bombs occur in AP-1 as in some other deposits, irregular bedding increasing toward the top. The top of AP-1—as of other fall deposits—is practically always variably eroded.

The main fan axis for all of L-AP-1 is directed to the northeast (Fig. 5a). Steep local dips of AP-1 suggest pre-eruptive or syn-eruptive faulting in several areas. Post-eruptive faulting is most spectacularly developed in the southward dipping slopes north of, and in the outskirts of Ahlat paralleling the northern boundary fault of Lake Van Basin.

Ignimbrite phase of AP-1 (M-AP-1: Middle Ahlat Pumice-1)

In several outcrops, about 2 km west of Ahlat as well as near Yolgözler (Fig. 7c in Sumita and Schmincke (2013a)), 25 km west-northwest of the center of Nemrut Caldera, fallout tephra AP-1 is overlain with slight unconformity by an ignimbrite generally <5 m thick and of identical mineralogical and chemical comenditic composition and age (ca. 190 ka). The thickness of the ignimbrite adjusts to slight depressions in the top of AP-1 fallout sheet, which we interpret to be due largely to syn-volcanic faulting. The AP-1 ignimbrite is locally strongly welded and the raw material for many of the colorful building blocks mined in small quarries ca. 8 km northwest of Ahlat.

Nemrut Formation (NF) (former Nemrut Depositional Unit (NDU) in Sumita and Schmincke (2013a))

We here replace the term Nemrut Depositional Unit (NDU) introduced by us (Sumita and Schmincke 2013a) to characterize the extraordinary complexity of volcanologically and compositionally highly variable eruptive and depositional events by the simpler term “Nemrut Formation (NF)”. NF consists of several contrasting mappable units and represents the most complex sequence of early fallout-surge-ignimbrite-agglutinate-surge-late fallout deposits found by us on the slopes of Nemrut Volcano. It reflects several intervals of evacuation from a magma reservoir compositionally zoned from large-volume peralkaline rhyolite to trachyte (Figs. 7, 8 and 9; Tables 1, 2). The depositional spectrum of the NF tephra deposits (fallout, ignimbrite, agglutinate), their mineralogy and chemistry (peralkaline trachytes and rhyolites) and ubiquitous magma mingling

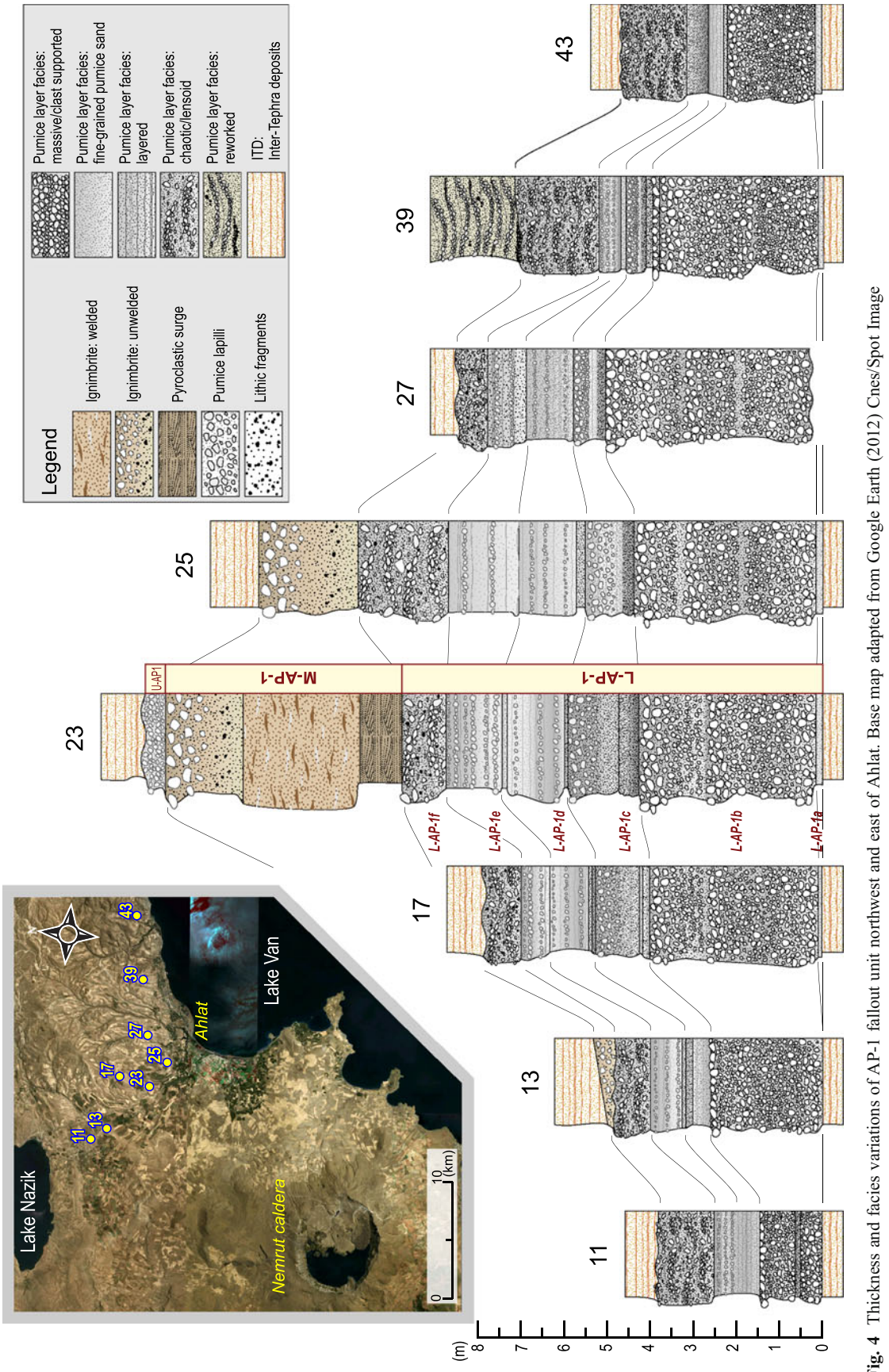

Fig. 4 Thickness and facies variations of AP-1 fallout unit northwest and east of Ahlat. Base map adapted from Google Earth (2012) Cnes/Spot Image

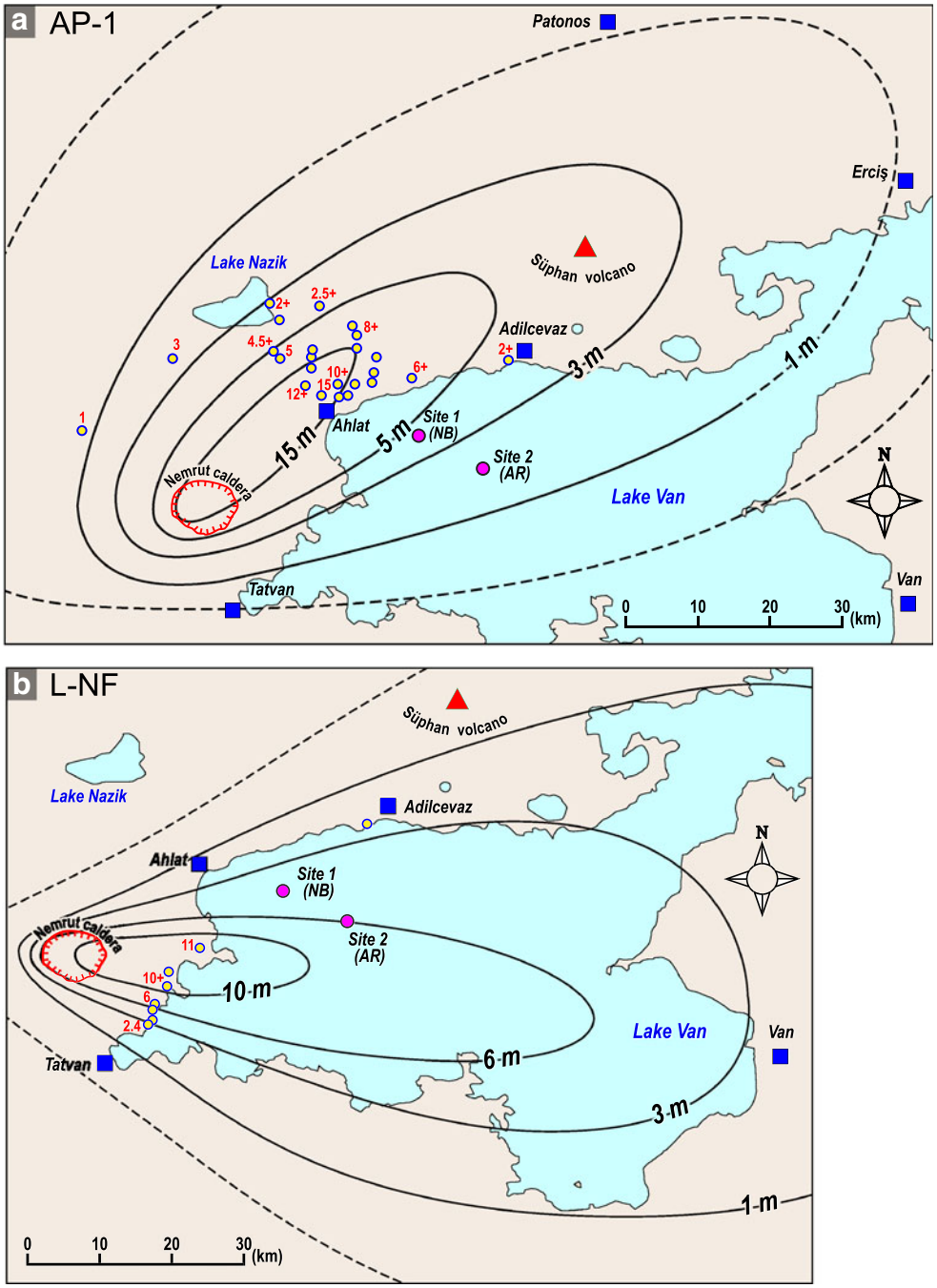

Fig. 5 Isopach maps of AP-1 (**a**) and L-NF (**b**). Thickness at individual localities in meters

are remarkably similar to those of the ca. 960 AD Baitoushan deposits (China/North Korea) (Horn and Schmincke 2000).

L-NF (Lower Nemrut Formation): Plinian fallout phase

We name as L-NF a basal rhyolitic Plinian fallout sheet, well exposed in ten sections between Şentepe and Halepkalesi mainly along the road Tatvan–Ahlat and locally near Adilcevaz. The well-sorted pumice lapilli deposit consists of two main subunits, L-NF1 and L-NF2, separated from one another by a <5-cm-thick tephra layer rich in colorful hydrothermally altered rock fragments. Both subunits change drastically but asymmetrically in thickness (Figs. 5b, 7), structures and grain size from south to north. In the southernmost road cut studied, L-NF1 is a 1.5 m thick normally size-graded fall layer with median grain size varying from 5 to 1 cm. The normal size grading disappears northward over 20 km while the grain size increases slightly, thickness remaining approximately constant. L-NF2, in

Fig. 6 Photographs showing subunit and medial facies of AP-1. **a** Subunit of main part of L-AP-1 (L-AP-1a to L-AP-1f) with eroded top (loc. 25, 5 km west of Ahlat). **b** Basal fine-grained subunit L-AP-1a (loc. 25). **c** L-AP-1 (>5 m thick) at village of Yuvadamı, 30 km NE of Nemrut (loc. 34)

contrast, thickens strongly from 0.2 m in the south (loc. 93) to ca. 12 m in the northernmost outcrop (loc. 72), a coarse-grained top layer, less than 15 cm thick in the south, gradually thickening drastically to the north. In the northernmost outcrop just west of Halepkalesi peninsula (loc. 72), L-NF2 can be subdivided into an extremely coarse-grained lower half with pumice bombs locally exceeding 50 cm (!) in diameter and a slightly finer-grained and vaguely bedded upper part L-NF3 with pumice lapilli/bombs 5–20 cm in diameter.

The very abrupt lateral change in grain size and thickness of L-NF2 suggests pronounced lateral shifts in relatively narrowly dispersed depositional lobes and a change from a steady eruption to a brief lithic-rich pulse, the fragmentation surface intersecting the hydrothermally altered lower conduit. The re-established eruption column culminated in powerful

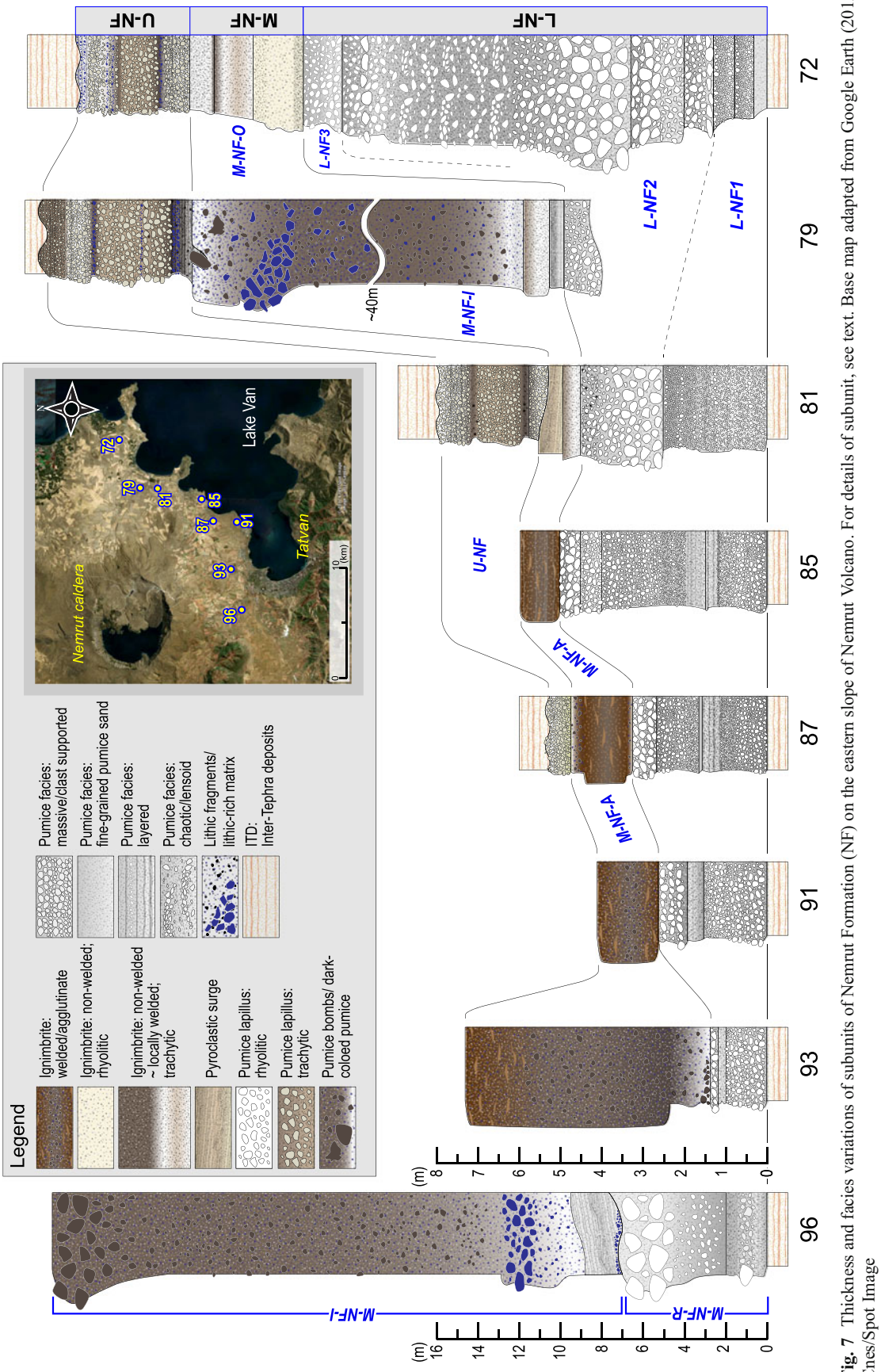

Fig. 7 Thickness and facies variations of subunits of Nemrut Formation (NF) on the eastern slope of Nemrut Volcano. For details of subunit, see text. Base map adapted from Google Earth (2012) Cnes/Spot Image

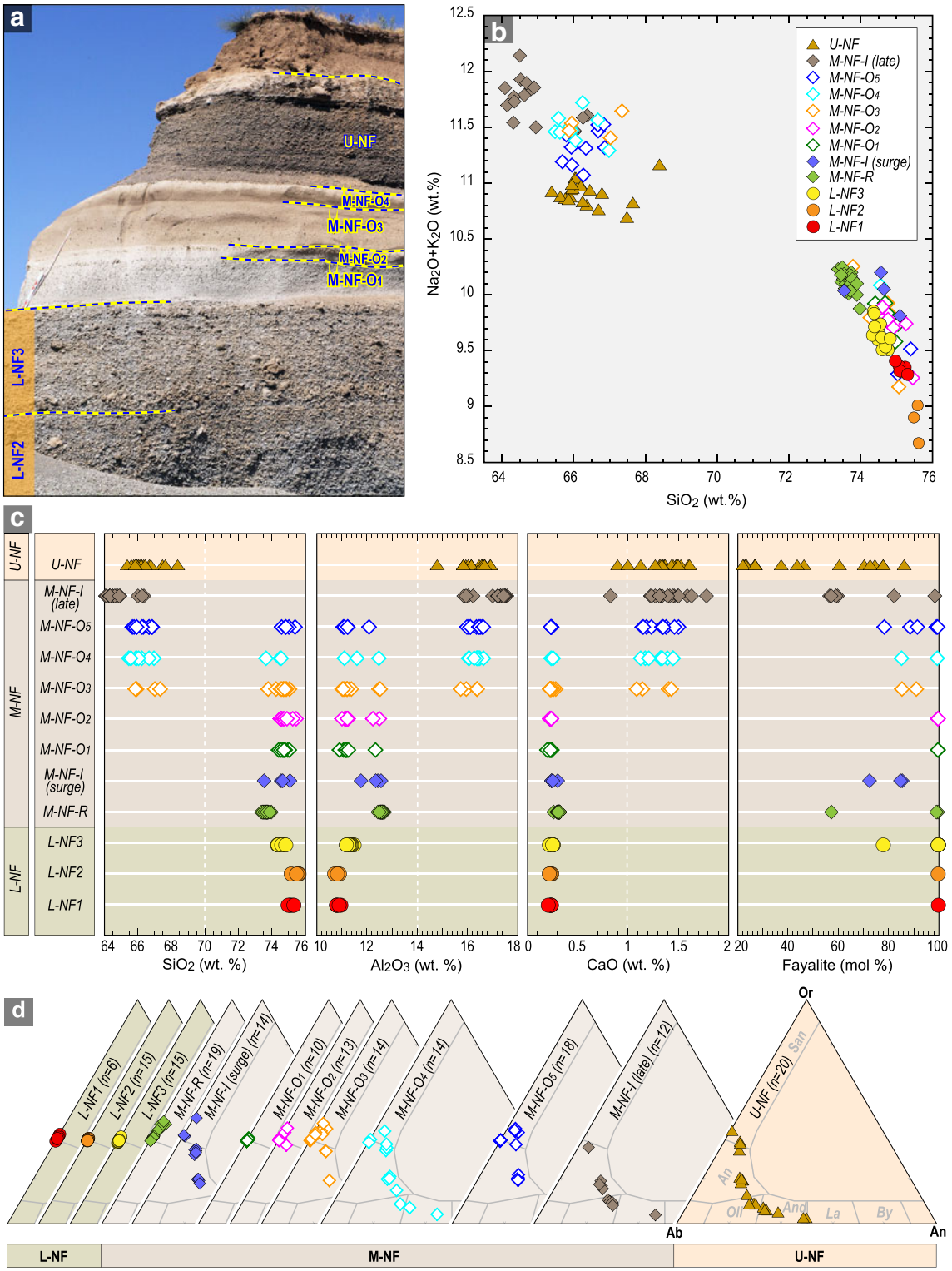

Fig. 8 **a** Nemrut Formation (NF) at Adabağ (loc. 72), west of Halepkalesi Peninsula showing stratigraphic section of top of rhyolitic L-NF fallout, overlain by M-NF ignimbrite overbank (L-NF-O) and final more mafic fallout deposit U-NF. The compositional contrast between subunits and major compositional gaps are well shown by EMP analyses of glass shards (selected major elements) (**b** and **c**), mol % fayalite (**c**) and feldspar phenocryst endmember compositions (**d**). Subunits were subdivided into several fall and flow units as shown in **a** and Fig. 7 (section of locality 72), also including the units not shown in **a** (e.g. M-NF-R (surge) and M-NF-I (surge): loc. 96, see also Figs. 7 and 9b; M-NF-I (late): loc. 94 and 79, later bomb-rich ignimbrite). Representative glass analyses of NF are shown in Table 2

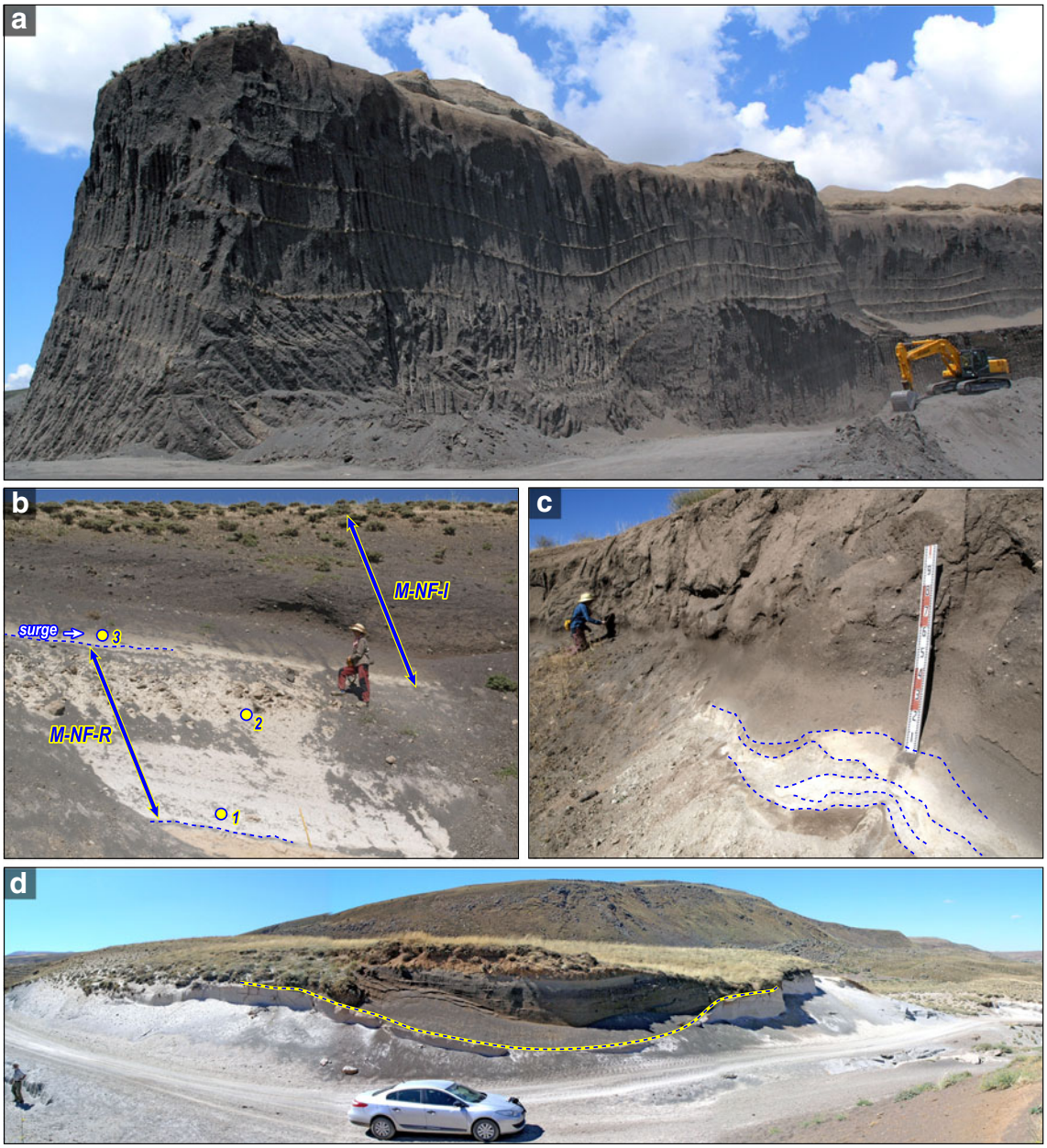

Fig. 9 **a** Black unwelded ca. 40 m thick NF pyroclastic flow deposit rich in variably vesiculated crystal-rich glassy bombs. Light-colored layers are zeolitized horizons reflecting groundwater levels not primary stratigraphy. Valley on eastern flank of Nemrut Volcano, 1 km south of Sarıkum (loc. 79). **b** Complex base of Nemrut Ignimbrite showing two rhyolitic basal layers. Part of the samples shown in Fig. 8 are taken from this locality: the lower one (*1* M-NF-R) layered, the upper one (*2* M-NF-R) very rich in lithic fragments, and a thin rhyolitic surge unit (*3* M-NF-I, surge) at the base of the main dark ignimbrite. **c** Complex rhyolitic, in part lithic-rich surge deposits underlying main dark brown Nemrut Ignimbrite ca. 2 km north of Güzelsu (loc. 52) **d** Up to 4 m thick white, very crystal-rich rhyolitic surge/flow deposit covered by dark relatively fine-grained Nemrut Ignimbrite. Ca. 1 km east of Güzelsu (loc. 53)

but highly unsteady eruptions, with the deposit axis strongly west–east oriented (Fig. 5b). The top of L-NF is variably eroded, locally possibly by surges heralding the next phase of the eruption. The fallout phase deposits (L-NF)—possibly the most voluminous of the eruption (depending on the still uncertain regional distribution of the M-NF)—are followed by amazingly complex pyroclastic flow and agglutinate deposits.

M-NF (Middle Nemrut Formation): Nemrut Ignimbrite

The youngest and best-exposed ignimbrite west, northwest and north of Tatvan is the central multi-facies ignimbrite of the Nemrut Formation, here called Nemrut Ignimbrite (M-NF). It corresponds in part to the Nemrut Ignimbrite of Karaoğlu et al. (2005) and most later authors, but has caused much confusion in the past as to its definition, correlation

Table 1 Major and trace element concentrations of selected rhyolite and trachyte tephras listed approximate by age

Analysis code:	175	153	50	124	152	76	19	37	81	120	27	47	28	29	158	121	109	115
Sample no.:	2010-09-03-02	2008-07-06-19	2009-07-16-03	2011-06-15-01	2008-07-06-17	2011-06-05-02	2009-07-15-01	2008-07-05-01	2011-06-08-08	2011-06-14-03	2009-07-18-06	2009-07-14-08	2009-07-18-08	2009-07-19-02	2009-07-14-04a	2011-06-14-05	2010-08-29-01	2010-09-01-09
Locality no.:	60	98	98	72	84	96	97	81	32	36	23	121	23	25	138	37	160	159
Tephra unit:	Obsidian lava 1441 AD	Holocene base surge tephra (NUS)	Çekmece Formation (Unit-3)	Lower Nemrut Formation (L-NF)	Middle Nemrut Formation (M-NF-A) (agglutinate)	Middle Nemrut Formation (M-NF-I) (glassy bomb)	Şentepe Pumice-1 (SP-1)	Halepkalesi Pumice-10 (HP-10)	Ahlat Pumice-8a (AP-8a)	Ahlat Pumice-5 (AP-5)	Ahlat Pumice-4b (AP-4b)	Tatvan Pumice (TP)	Ahlat Pumice-2 (AP-2)	Ahlat Pumice-1 (L-AP-1)	Küçüksu Ignimbrite (KCI)	Selaviat Tepe Pumice-1 (STP-1)	Patnos Pumice (Süphan)	Kömrütlü Pumice (Süphan)
Rock type:	CR	CR	T	CR	T	T	T	T	CR	T	PR	CR	CR	CR	T	T	R	R
Major elements (*wt.%*)																		
SiO_2	72.95	68.74	61.68	70.64	62.94	62.78	59.04	60.46	69.74	58.47	67.15	67.92	68.84	68.08	64.80	63.56	72.43	69.24
TiO_2	0.15	0.22	0.87	0.24	0.47	0.40	0.40	0.29	0.24	0.42	0.39	0.27	0.19	0.25	0.32	0.28	0.07	0.24
Al_2O_3	12.13	11.85	16.34	10.53	17.34	16.72	15.72	15.98	10.40	16.35	9.80	12.20	12.65	11.36	14.58	15.23	12.64	14.37
Fe_2O_3	2.33	3.54	6.54	4.49	4.31	3.98	6.06	4.97	4.36	6.25	6.80	4.89	2.43	3.99	4.18	4.14	1.32	2.47
MgO	0.03	0.01	0.81	0.01	0.31	0.21	0.19	0.14	0.02	0.35	0.01	0.04	0.05	0.02	0.06	0.08	0.04	0.32
CaO	0.32	0.34	2.94	0.29	1.35	1.84	0.92	0.69	0.32	1.15	0.47	0.41	0.54	0.42	1.20	1.11	0.42	1.46
Na_2O	4.93	4.93	5.26	4.87	6.76	5.83	6.68	6.40	4.85	6.96	5.12	5.05	4.08	4.98	4.61	5.00	3.61	4.09
K_2O	4.55	4.64	3.74	4.35	5.11	4.68	4.87	5.11	4.45	4.96	4.53	4.71	5.55	4.50	5.55	5.67	5.11	4.13
P_2O_5	0.01	0.01	0.25	0.01	0.09	0.07	0.05	0.04	0.01	0.08	0.02	0.01	0.01	0.02	0.03	0.03	0.01	0.06
MnO	0.06	0.08	0.13	0.10	0.12	0.14	0.19	0.14	0.10	0.18	0.17	0.11	0.08	0.11	0.12	0.10	0.07	0.06
SO_3	0.00	0.01	0.03	0.00	0.02	0.02	0.03	0.03	0.03	0.01	0.04	0.02	0.01	0.01	0.03	0.00	0.01	0.01
H_2O^+			0.90				3.86	4.52			3.90	4.25	3.53	4.04				
H_2O^-			0.18				0.85	0.53			0.45	0.43	0.36	0.35				
LOI	0.45	3.36		4.30	0.21	1.89			3.90	3.87					2.89	4.32	4.22	3.71
Total	97.91	97.73	99.68	99.83	99.03	98.56	98.87	99.29	98.42	99.05	98.85	100.30	98.32	98.13	98.37	99.52	99.95	100.16
P.I.	1.07	1.11	0.78	1.21	0.96	0.88	1.03	1.00	1.23	1.03	1.36	1.10	1.01	1.15	0.93	0.94	0.91	0.78
Trace elements (*ppm*)																		
V	7	3	26	2	2	4	0	5	0	8	0	4	3	6	0	0	5	3
Cr	18	17	0	16	11	14	3	0	16	21	0	7	6	0	20	20	19	18
Co	4	6	6	0	2	3	0	2	6	3	4	0	0	0	4	3	2	1
Ni	3	2	2	0	0	0	4	3	0	2	2	3	1	3	1	5	0	0
Cu	0	0	3	0	2	0	10	0	0	0	0	2	0	0	0	0	0	0
Sc	7	4	13	6	6	12	0	10	0	0	7	5	9	0	4	8	4	0
Ba	15	9	645	9	590	839	11	0	19	76	17	19	33	31	697	147	44	474
Sr	12	8	205	3	91	122	31	4	2	31	8	10	4	9	49	13	19	82
Zn	123	151	93	185	79	62	178	123	183	127	233	181	88	183	114	106	68	51
Ga	31	32	19	27	25	19	35	27	24	23	31	31	27	30	33	22	14	13
Rb	184	213	105	221	110	63	221	181	206	170	211	228	211	183	153	186	178	146
Y	104	107	49	129	42	32	107	64	127	71	138	126	91	112	67	67	56	40

Table 1 (continued)

Analysis code:	175	153	50	124	152	76	19	37	81	120	27	47	28	29	158	121	109	115
Sample no.:	2010-09-03-02	2008-07-06-19	2009-07-16-03	2011-06-15-01	2008-07-06-17	2011-06-05-02	2009-07-15-01	2008-07-05-01	2011-06-08-08	2011-06-14-03	2009-07-18-06	2009-07-14-08	2009-07-18-08	2009-07-19-02	2009-07-14-04a	2011-06-14-05	2010-08-29-01	2010-09-01-09
Locality no.:	60	98	98	72	84	96	97	81	32	36	23	121	23	25	138	37	160	159
Tephra unit:	Obsidian lava 1441AD	Holocene base surge tephra (NUS)	Çekmece Formation (Unit-3)	Lower Nemrut Formation (L-NF)	Middle Nemrut Formation (M-NF-A) (agglutinate)	Middle Nemrut Formation (M-NF-I) (glassy bomb)	Şentepe Pumice-1 (SP-1)	Halepkalesi Pumice-10 (HP-10)	Ahlat Pumice-8a (AP-8a)	Ahlat Pumice-5 (AP-5)	Ahlat Pumice-4b (AP-4b)	Tatvan Pumice (TP)	Ahlat Pumice-2 (AP-2)	Ahlat Pumice-1 (L-AP-1)	Küçüksu Ignimbrite (KCI)	Selaviat Tepe Pumice-1 (STP-1)	Patnos Pumice (Süphan)	Kömrütlü Pumice (Süphan)
Rock type:	CR	CR	T	CR	T	T	T	T	CR	T	PR	CR	CR	CR	T	T	R	R
Nb	61	65	27	75	31	22	97	57	73	61	71	76	57	66	42	51	30	15
La	90	96	41	138	41	23	117	72	115	74	104	115	89	97	80	76	28	44
Ce	141	197	74	226	80	42	188	122	212	125	189	192	167	165	128	126	58	67
Zr	682	1070	466	1216	470	285	1526	847	1179	898	1234	1308	524	1100	707	883	255	269
Nd	65	89	32	93	38	22	67	48	94	49	72	68	63	60	61	51	31	34
Pb	27	35	14	32	18	10	41	20	42	39	33	34	21	27	16	25	31	15
U	13	9	0	9	4	0	10	9	11	5	5	12	7	6	4	6	6	3
Th	21	28	16	28	11	0	40	17	27	13	29	29	26	26	12	15	16	6
Zr/Nb	11.2	16.5	17.3	16.2	15.2	13.0	15.7	14.9	16.2	14.7	17.4	17.2	9.2	16.7	16.8	17.3	8.5	17.9

Most tephras represent pumice lapilli from fallout deposits except for No. 175 (historic obsidian lava flow) and -158, -152, -76 (ignimbrites). Most samples are from Nemrut Volcano except for No. 109 and -115 that are sourced in Süphan Volcano. More detailed information on localities is given in Sumita and Schmincke (2013a). XRF analyses were carried out by Mineralogisch-Petrographisches Institut Universität Hamburg

CR comenditic rhyolite; *PR* pantelleritic rhyolite; *R* rhyolite; *T* Trachyte

Table 2 Representative EMP analyses of glass shards in subunits of NF

Unit:	U-NF	M-NF-I (late bombs)	M-NF-O_5	M-NF-O_5	M-NF-O_4	M-NF-O_4	M-NF-O_3	M-NF-O_3	M-NF-O_2	M-NF-O_1	M-NF-I (surge)	M-NF-R	L-NF3	L-NF-2	L-NF-1
Locality:	81	79	72	72	72	72	72	72	72	72	96	96	72	81	81
Sample No.:	2008-07-05-07	2008-07-05-09	2008-07-05-12	2008-07-05-12	2008-07-05-13	2008-07-05-13	2008-07-05-14	2008-07-05-14	2008-07-05-15	2008-07-05-16	2008-07-06-20	2008-07-06-21	2008-07-05-17	2008-07-05-05	2008-07-05-03
Glass type and grain No.:	cgl-8	cgl-4	l br gl-7	cgl-8	br gl-9	cgl-2	l br gl-11	cgl-9	cgl-5	cgl-6	d br gl-6	dgl-7	cgl-3	cgl-2	cgl-5
Number of analyses:	2	1	2	1	2	2	2	2	2	2	2	2	2	3	3
(*wt* %)															
SiO_2	65.62	64.86	66.29	74.21	66.02	73.12	65.90	74.22	74.60	74.51	73.68	73.64	73.29	72.71	73.39
TiO_2	0.51	0.40	0.38	0.27	0.41	0.23	0.43	0.25	0.26	0.24	0.16	0.21	0.24	0.25	0.26
Al_2O_3	16.61	15.96	16.02	11.16	16.38	10.90	16.38	11.22	11.25	11.15	12.29	12.63	11.21	10.44	10.61
FeO*	4.26	3.93	3.78	3.57	4.00	3.93	3.84	4.10	3.80	3.91	2.31	2.95	3.80	4.02	3.84
MnO	0.21	0.16	0.09	0.09	0.17	0.13	0.16	0.12	0.06	0.08	0.03	0.07	0.11	0.10	0.08
MgO	0.30	0.22	0.17	0.01	0.20	0.00	0.21	0.00	0.01	0.01	0.01	0.00	0.00	0.00	0.02
CaO	1.34	1.37	1.23	0.24	1.34	0.25	1.41	0.23	0.24	0.22	0.24	0.31	0.23	0.23	0.20
Na_2O	5.58	5.57	5.96	5.20	5.97	4.62	6.45	4.94	5.36	5.50	4.97	5.37	5.30	4.74	4.64
K_2O	5.27	5.70	5.44	4.42	5.41	4.95	5.09	4.85	4.42	4.38	5.11	4.71	4.24	4.27	4.41
P_2O_5	0.10	0.07	0.05	0.01	0.05	0.01	0.07	0.01	0.00	0.00	0.02	0.01	0.01	0.00	0.01
Total:	99.77	98.25	99.40	99.18	99.96	98.13	99.92	99.93	99.99	99.98	98.81	99.91	98.40	96.76	97.46
Na_2O+K_2O	10.87	11.47	11.47	9.70	11.38	9.75	11.54	9.80	9.78	9.88	10.20	10.09	9.69	9.31	9.29

Abbreviations for glass types: *br gl* brown glass; *cgl* clear glass (transparent, no color); *d br gl* dark brown glass; *l br gl* light brown glass

and areal distribution. It is exposed close to Tatvan and thus visited frequently by geologists. This deposit is an impressive example of the complex generation, transport and deposition of pyroclastic density current tongues varying widely in mode of eruption and emplacement temperature, grain size, thickness, volume, areal distribution, composition etc. Correlation of this mass flow deposit even over distances of less than 1 km was exceedingly difficult initially. Moreover, the various flow facies are underlain by the major rhyolitic fallout sheet (L-NF) and overlain by a trachyte late stage fallout sheet (U-NF) of lesser volume, all together representing one eruptive episode.

We recognize at least four distinct, highly contrasting facies types of M-NF, some locally restricted (proximal surge, thick valley-confined unwelded, locally welded, agglutinate and thin fine-grained overbank on interfluves). Different flow units also differ in phenocryst mineralogy (Fig. 8).

1. Upper slope facies: A generally poorly to slightly welded reddish-brown massive deposit, commonly <2 m thick crops out in scattered road side outcrops between the Nemrut Caldera rim and the village of Çekmece. This unit may correspond to the "Kantaşi Ignimbrite" of Çubukçu et al. (2012) and Ulusoy et al. (2012).
2. Middle slope to upper plateau facies: A moderately welded, valley-filling ca. 6 m thick ignimbrite in the center of the village of Çekmece (at least three flow units) represents local intracanyon thickening. A valley-confined tongue marked at the top by impressive grooves engraved over the centuries by cartwheels continues south of the village for ca. 1 km in Seymiran Valley. The gently sloping terrain between Ahlat and the village of Serinbayır at the foot of Nemrut cone is underlain by a poorly welded columnar-jointed facies of this ignimbrite.
3. The lower slope or lower plateau facies, locally exposed in road cuts, quarries and ravines for some 20 km, is represented by basically four subfacies:

Subfacies-1 (M-NF-R) A basal light-colored, apparently entirely rhyolitic, locally extremely lithic-rich, in part crystal-rich, crudely layered to locally surge-like or massive facies up to 4 m thick occurs at the base of a black bomb-rich thick flow as in Seymiran valley (Fig. 9b). We interpret this complex deposit as preceding the main dominantly trachytic flow phase of M-NF. We speculate that pockets of rhyolite magma that had remained in the reservoir following L-NF eruption were flushed out by the ensuing M-NF eruption of dominantly trachytic magma. The abundance of rock fragments probably reflects conduit collapse caused by the eruption of the large-magnitude L-NF.

Subfacies-2 (M-NF-I) A valley-ponded unwelded black ignimbrite facies, up to ca. 40 m thick, heavily quarried in several canyons west of Tatvan and between Sarıkum and Kıyıdüzü, consists of black pumice lapilli and bombs up to 30 cm in diameter and represents the bulk of the ignimbrite in the sector Tatvan–Sarıkum (Fig. 9a). The deposit can be subdivided into several flow units differing in grain size, grading and welding. The great thickness of the valley-

ponded facies shows that the pre-NF terrain was highly irregular with deeply carved canyons opening into lake Van. The present gently undulating surface morphology is largely the result of smoothing over by the M-NF pyroclastic flows. Evidence of magma mingling (streaky pumice and compositionally contrasting lapilli and corroded feldspar phenocrysts) is common, the relative proportion of trachytic and rhyolitic components being highly variable. The dominant composition is trachyte but the overall black deposit color is due to the abundance of glassy material (obsidian) in lapilli and bombs. Spectacular vapor-phase cemented degassing pipes are aligned on the southern slopes of a small canyon just north of the road Tatvan-Çekmece (Fig. 9a in Sumita and Schmincke (2013a)).

Subfacies-3 Agglutinate phase (M-NF-A): A compact, columnar, brownish to burgundy-colored, generally ca. 2-m-thick sheet of moderately welded tephra directly overlies the basal fallout tephra L-NF in several road cuts for ca. 10 km between the outskirts of Tatvan and the village of Kıyıdüzü (Fig. 7) as well as along the northeastern slope of Nemrut cone where welding is less pronounced. This blanket consists of about 3 subunits with indistinct boundaries that may correspond to the 3 flow units of M-NF in Çekmece village. The unit roughly maintains its thickness even where the local dip is steep as in Simek Bay (south of loc. 85). The regionally nearly constant thickness of this unit across strike over a hilly terrain resembles that of a fall deposit but welding provides proof that the deposit was emplaced hot. We interpret this facies as agglutinate deposited from lava fountains. The agglutinate blanket is transitional south and northeast to the ca. 6-m-thick moderately welded ignimbrite (subfacies 2 above) in the village of Çekmece and to welded ignimbrite exposed in small ravines west of the former Tatvan city dump (Fig. 7, loc. 93).

Subfacies-4 Overbank facies (M-NF-O). Completely unwelded, soft, friable, massive fine-grained ash deposits, up to 2 m thick with a common light brown "cappuccino" hue overlie L-NF, e.g. at locality 72 (Figs. 7, 8). This thin interval presents in a nutshell the striking compositional gradation of the main valley-ponded deposit. The lower rhyolitic white part is possibly correlative to the white surge deposit at the base of the main black ignimbrite (Fig. 9b) while the compositionally and mineralogically more primitive brown massive ash corresponds to the top of the black bomb-rich facies. At slightly higher elevations, M-NF-O is represented by a surge facies (loc. 81) (Fig. 9b in Sumita and Schmincke (2013a)).

U-NF (Upper Nemrut Formation): Terminal (upper) fallout phase

An extremely lithic-rich, up to 3 m thick coarse fall and surge deposit consisting of darker and denser trachytic pumice and rather denser pumice caps the fine-grained overbank deposits (Figs. 8a and 9c in Sumita and Schmincke (2013a)), the abundance of lithics apparently reflecting final clearing of the collapsed conduit (caldera).

Regional distribution of NF

We found the equivalent of Nemrut Ignimbrite around the village of Güzelsu ca. 15 km north of the center of Nemrut Caldera. Here, the basal rhyolitic subfacies M-NF-R is represented by white crystal-rich surge deposits up to 4 m thick overlain with a relatively sharp boundary by a massive trachytic ignimbrite distinctly finer-grained than south of Nemrut Volcano (Figs. 9c, d). West of Nemrut Volcano, the uppermost of several ignimbrites that leveled out Muş Basin may correspond to M-NF-I that also appears to have climbed the eastern side of morphologically prominent elongate Mazik Dome. If this areal distribution is confirmed, the total volume of the ignimbrite may be similar in magma volume (DRE) to the basal rhyolite "fall deposit", which is a reworked facies consisting of pumice lapilli ca. 1 cm in diameter (Mager personal comm.) at Van, 140 km due east of Nemrut Volcano. In any case, the total magma volume of the ca. 30 ka Nemrut Formation deposits may exceed 10 km^3 DRE.

Mineral and chemical compositions

Below, we briefly summarize the main mineralogical and chemical characteristics of the tephra deposits mainly of Nemrut but also of locally interlayered Süphan tephras that fortunately differ significantly in composition from Nemrut tephra (Sumita and Schmincke 2009, 2012). This summary is based on 140 whole rock (single large lapilli or several adjacent lapilli) major and trace element analyses (Table 1 this paper; Table 2 in Sumita and Schmincke (2013b)) and several tens of thousands of EMP analyses (> 60 Nemrut and Süphan tephra units) of glass shards (e.g. Table 2) and feldspar (Table 3), clinopyroxene (Table 4) and olivine phenocrysts (Table 5), as well as selected glass inclusions; a more in-depth petrological evaluation will be presented elsewhere. Previously published chemical analyses of Nemrut rocks (Pearce et al. 1990; Yılmaz et al. 1998; Özdemir et al. 2006; Çubukçu et al. 2012) are practically all of lavas or intrusions and most lack published documentation of localities, elevation, stratigraphy, and mineralogy.

Özdemir et al. (2006) listed plagioclase, clinopyroxene, olivine and amphibole as the major phases in Nemrut magmas joined by K-feldspar, biotite and apatite in the fractionating assemblages during the course of magmatic

Table 3 Representative EMP analyses of feldspar phenocrysts from Nemrut and Süphan tephra deposits

Source:	Nemrut								Süphan				
Tephra unit:	AP-1 (L-AP-1b)	AP-2	AP-3	AP-4a	AP-4b	AP-5	AP-6	AP-8a	Erciş Pumice	Patnos Pumice	Patnos Pumice	Kömrütlü Pumice	Kömrütlü Pumice
Rock type:	CR-PR	CR	CT	PR	PR	T	T	CR	R	R	R	R	R
Locality:	25	23	23	23	23	25	25	26	166	162	162	159	159
Sample no.:	2008-07-06-06	2009-07-18-08	2009-07-18-04	2009-07-18-05	2009-07-18-06	2008-07-06-10	2008-07-06-11	2008-07-06-14	2008-07-08-04	2010-08-29-05	2010-08-29-05	2010-09-01-08	2010-09-01-08
Grain no.:	fp-2	fp-10	f-p18	fp-8	fp-11	fp-9	fp-1	fp-8	fp-8	fp-3	fp-1	fp-1	fp-19
Number of analyses:	4	2	2	2	2	2	4	3	3	2	2	2	2
(*wt*. %)													
SiO_2	67.30	66.24	66.89	67.09	67.36	66.17	67.28	67.11	61.32	65.49	65.64	65.02	65.75
TiO_2	0.02	0.03	0.02	0.01	0.01	0.02	0.03	0.01	0.00	0.01	0.00	0.01	0.00
Al_2O_3	19.56	19.77	18.99	18.78	18.74	20.73	19.60	18.98	24.04	22.11	19.23	22.62	19.36
FeO*	0.34	0.21	0.32	0.48	0.68	0.21	0.53	0.46	0.15	0.05	0.06	0.09	0.06
MgO	0.00	0.00	0.00	0.00	0.00	0.00	0.00	0.00	0.00	0.00	0.00	0.00	0.00
CaO	0.07	0.45	0.05	0.00	0.01	0.56	0.06	0.03	4.96	2.48	0.21	3.20	0.19
Na_2O	6.73	6.27	6.31	6.59	6.98	6.06	6.47	6.86	7.28	8.42	3.52	7.93	3.46
K_2O	6.06	6.69	7.08	6.76	6.13	6.89	6.15	5.97	0.89	1.43	11.00	1.34	11.21
Total:	100.08	99.66	99.64	99.71	99.91	100.63	100.12	99.42	98.64	99.98	99.66	100.19	100.02
Or	37.1	40.3	42.4	40.3	36.6	41.6	38.4	36.3	5.5	8.7	66.6	8.3	67.4
Ab	62.6	57.4	57.4	59.7	63.4	55.6	61.3	63.5	68.6	78.5	32.3	75.0	31.6
An	0.3	2.3	0.2	0.0	0.0	2.8	0.3	0.2	25.9	12.8	1.1	16.7	1.0

Table 4 Representative EMP analyses of clinopyroxene phenocrysts from Nemrut and Süphan tephra deposits

Source:	Nemrut											Süphan
Tephra unit:	AP-1 (L-AP-1b)	AP-2	AP-3	AP-3	AP-4a	AP-4b	AP-5	AP-6	AP-6	AP-8a	AP-8a	Erciş Pumice
Rock type:	CR-PR	CR	CT	CT	PR	PR	T	T	T	CR	CR	R
locality:	25	23	23	23	23	23	25	25	25	25	25	166
Sample no.:	2008-07-06-06	2009-07-18-08	2009-07-18-04	2009-07-18-04	2009-07-18-06	2009-07-18-05	2008-07-06-10	2008-07-06-11	2008-07-06-11	2009-07-19-04	2009-07-19-04	2008-07-08-04
Grain no.:	px-6	px-8	px-4	px-7	px-17	px-3	px-1	px-2	px-5	px-1	px-14	px-1
Number of analyses:	2	2	2	2	2	2	2	2	2	2	2	2
(*wt*. %)												
SiO_2	48.94	49.62	48.70	48.81	48.52	48.73	48.94	49.54	48.84	48.95	51.75	49.30
TiO_2	0.25	0.24	0.37	0.40	0.31	0.42	0.55	0.18	0.43	0.28	0.42	0.09
Al_2O_3	0.17	0.41	0.29	0.32	0.20	0.41	0.85	0.24	0.30	0.17	0.96	0.42
Cr_2O_3	0.01	0.01	0.00	0.02	0.00	0.00	0.02	0.00	0.00	0.00	0.00	0.03
FeO*	29.67	25.95	29.52	30.05	29.20	28.17	26.28	28.17	28.74	30.44	14.36	38.16
MnO	1.36	1.33	1.23	1.30	1.13	1.22	1.33	1.23	1.51	1.13	0.69	1.86
MgO	0.28	3.74	0.57	0.53	0.37	1.38	2.15	1.71	0.70	0.14	11.35	9.80
CaO	18.63	19.01	19.33	18.58	18.98	19.96	19.82	19.15	19.46	18.36	20.69	1.08
Na_2O	0.83	0.43	0.75	0.80	1.09	0.52	0.51	0.58	0.65	1.22	0.45	0.03
K_2O	0.01	0.00	0.00	0.01	0.00	0.00	0.00	0.00	0.00	0.00	0.00	0.00
NiO	0.01	0.02	0.01	0.05	0.01	0.00	0.01	0.03	0.01	0.02	0.04	0.00
Total:	100.15	100.77	100.77	100.86	99.81	100.81	100.44	100.83	100.64	100.70	100.70	100.76
En	0.9	11.4	1.8	1.7	1.2	4.3	6.7	5.4	2.2	0.5	32.8	29.7
Fs	56.0	46.8	54.3	42.5	54.7	51.1	48.6	51.6	53.6	56.9	24.3	68.0
Wo	43.1	41.8	43.9	55.8	44.1	44.6	44.7	43.1	44.2	42.6	42.9	2.4

Table 5 Representative EMP analyses of olivine phenocrysts from Nemrut tephra deposits

Tephra unit:	AP-1 (L-AP-1a)	AP-2	AP-3	AP-4b	AP-8a	U-NF	Holocene surge deposits
Rock type:	CR	CR	CT	PR	CR	CT	CR
Locality no.:	21	23	23	23	25	81	100
Sample no.:	2009-07-20-05	2009-07-18-08	2009-07-18-04	2009-07-18-05	2008-07-06-12	2008-07-05-07	2008-07-03-03
Grain no.:	ol-2	ol-4	ol-19	ol-9	ol-1	ol-3	ol-3
Number of analyses:	2	2	2	2	2	2	2
(*wt.* %)							
SiO_2	30.41	30.87	30.47	30.20	30.69	38.35	29.72
Al_2O_3	0.00	0.00	0.00	0.00	0.00	0.04	0.00
FeO*	66.11	63.82	64.64	66.73	65.74	21.57	65.34
MnO	4.04	3.70	3.72	3.46	3.15	0.35	2.94
MgO	0.11	2.44	1.41	0.24	0.07	40.49	0.40
NiO	0.00	0.00	0.00	0.00	0.00	0.07	0.00
CaO	0.37	0.32	0.61	0.27	0.31	0.27	0.27
Cr_2O_3	0.01	0.01	0.00	0.00	0.00	0.02	0.00
Total	101.05	101.14	100.85	100.90	99.96	101.14	98.67
Fo	0.3	6.1	3.5	0.6	0.2	76.7	1.0
Fa	99.7	94.0	96.5	99.4	99.8	23.3	99.0

differentiation. Nemrut Ignimbrite was said to be characterized by sanidine, plagioclase, clinopyroxene and hornblende (Karaoğlu et al. 2005). Çubukçu et al. (2007; 2012) point out that Nemrut volcanic deposits are dominated by silica-saturated peralkaline rocks, plagioclase-bearing units representing only a small fraction and being restricted to mafic compositions. Moreover, they found anorthoclase—rather than sanidine—to be the major K-feldspar, with olivine ranging widely in composition up to fayalite and occurring in all eruptive units of Nemrut; amphibole is restricted to pre-caldera rocks. They also did not find biotite but aenigmatite and chevkinite. Çubukçu et al. (2007; 2012) also agreed with Pearce et al. (1990) on the peralkaline nature of the felsic magmas of Nemrut.

We have recognized several contrasting mineral assemblages in the >60 tephra units (Nemrut and Süphan) studied by us (Figs. 10, 11). Feldspar phenocrysts, chiefly anorthoclase ($Or_{30–46}$) dominate. Ternary feldspars or plagioclase, generally strongly corroded, are most prominent in trachyte fall deposits and ignimbrites in which feldspars are commonly highly fragmented and corroded due to mixing of more mafic (trachytic) with rhyolitic magma during later stages of an eruption (Fig. 10b). Most of the trachytic and rhyolitic tephra layers contain Fe-rich green clinopyroxene close to *hedenbergite* in composition (Fig. 10a, f), lesser augite and most also Fe-rich olivine to *fayalite* (Fig. 10a) apart from Fe-Ti-oxides. Colorless to light brown, generally somewhat corroded augitic clinopyroxene occurs especially in some trachytic tephras and in the slightly more mafic ignimbrites. Aenigmatite occurs in distinct phenocryst assemblages: (1) aenigmatite + quartz next to the dominating anorthoclase, (2) aenigmatite + Fe-rich clinopyroxene, + quartz, and (3) aenigmatite + hedenbergite + fayalitic olivine with anorthoclase as only felsic phenocryst. Accessory aenigmatite occurs, e.g., in units AP-3 and AP-6 and minor quartz in some units. Apatite generally attached to Fe-rich clinopyroxene is common. Chevkinite and zircon are rare accessories. Alkali amphibole occurs exclusively in sub-volcanic/plutonic rock fragments in several tephra deposits but never as phenocryst.

Nemrut tephras range from rare mugearitic and moderately mafic trachyte to highly evolved rhyolite; intermediate compositions are all but absent. Many Nemrut tephras are slightly to moderately peralkaline (comenditic to rarely pantelleritic) (Fig. 11). We distinguish high-Si from low-Si trachytes.

Basalts are a rare commodity in the felsic Nemrut system and comprise a couple of scoria deposits near the base of the tephra succession (older than AP-1) plus the lava flows (loc. 61, 62) erupted in 1441 from a fissure just north of the caldera (Fig. 11; photograph see Fig. 8a in Sumita and Schmincke (2013a)). All basalt compositions are moderately evolved (MgO generally <7.0 wt. %, Cr and Ni ppm <80) mildly alkaline basalts commonly with <2 vol.% olivine phenocrysts and microphenocrysts and <1 vol.% of plagioclase. The basalts of the huge, dominantly hyaloclastite İncekaya system, whose eruptive center was located far outside Nemrut edifice, are high alumina basalts.

Süphan tephras are generally easy to distinguish petrographically, mineralogically and chemically from Nemrut tephras (Sumita and Schmincke 2009) (Fig. 10; Tables 3, 4, 6). Macroscopically, small vesicles and distinctly white color characterize pumice of rhyolitic tephras sourced in

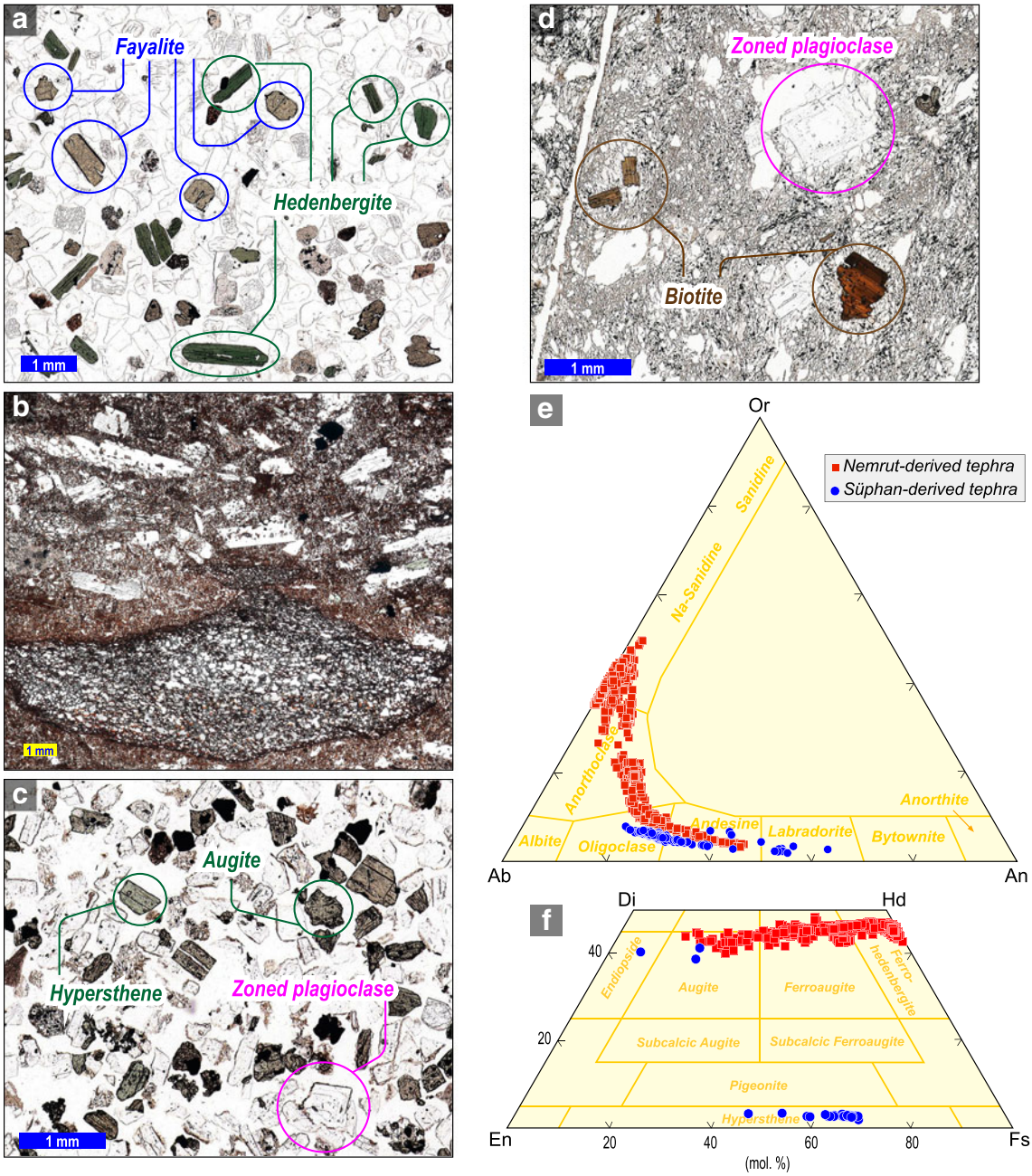

Fig. 10 Thin section photomicrographs of grain mounts of Nemrut (**a** and **b**) and Süphan (**c** and **d**) tephra layers. **a** Grain mount of AP-3 (loc. 23). **b** M-NF-A: Thin section of agglutinate unit of the M-NF (loc. 84). Note flattened trachytic lapillus and strongly corroded plagioclase feldspar crystals in upper half of photomicrograph. **c** Pumice from fallout deposits from canyon bottom north of Aygil Maar on the ca. 2,000 m asl southern slope of Süphan Volcano (loc. 156) **d** Erciş Pumice at Çelebibağı southwest of Erciş (loc. 156). **e** Ternary feldspar diagram showing contrast in feldspar compositions of Nemrut compared to Süphan tephras. **f** Pyroxene quadrilateral showing contrast between Nemrut and Süphan compositions

Süphan. Chemically, Süphan rhyolites are high silica, subalkaline and are characterized by lower TiO_2 and FeO*, slightly lower total alkalis, mostly slightly higher K_2O/Na_2O-ratios and higher SiO_2 and CaO concentrations compared to Nemrut compositions. Incompatible trace element concentrations of, e.g., Zr, Nb, Ce, La, Ga and others are lower than in Nemrut tephras at similar SiO_2-concentrations while Sr and Ba-concentrations are generally significantly higher. Hypersthene, clinopyroxene and lesser olivine are the major mafic phenocryst phases (Fig. 10c). Hydrous crystals are biotite alone, or with rare amphibole and/or hypersthene in many evolved tephras (Fig. 10d) while others contain only two pyroxenes and olivine. Chevkinite is a common accessory phase in compositionally

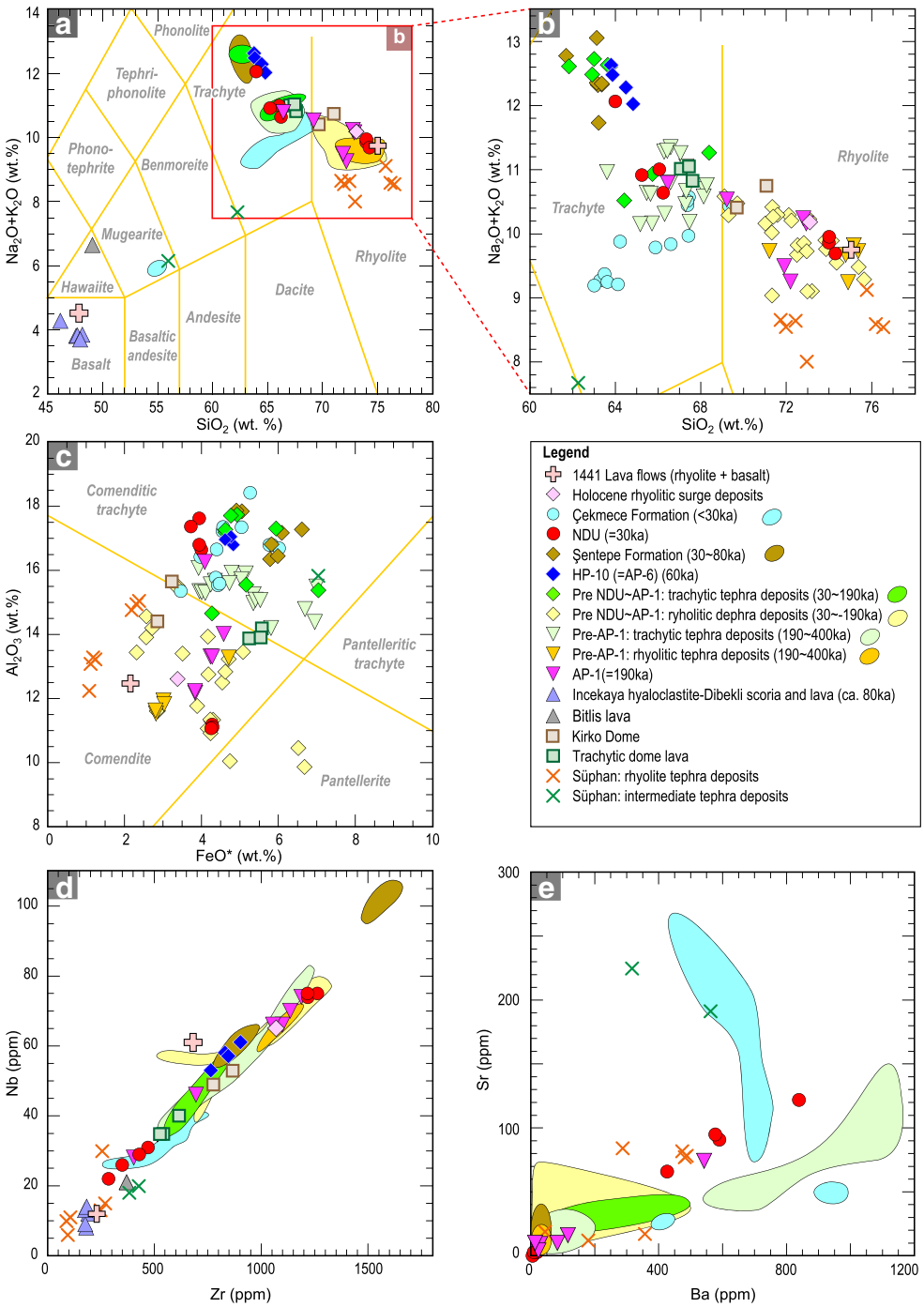

Fig. 11 Harker variation diagram (Le Bas et al. 1986) showing nomenclature of Nemrut and minor Süphan tephra bulk rock pumice compositions (**a** and **b**). Also shown are the fields for peralkaline compositions (**c** Macdonald 1974), and trace element concentrations of Zr vs. Nb (**d**) and Ba vs. Sr (**e**). Stratigraphically coherent trachyte groups are shown by different color symbols and also as a field in case the symbols are too dense. For details, see text. Representative analyses are shown in Table 1 (this paper) and Table 2 in Sumita and Schmincke (2013b), and will be discussed fully in a petrological account of Nemrut Volcano magma evolution (in prep)

highly evolved Süphan rocks. Corrosion and complex intergrowths characterize pyroxene phenocrysts with plagioclase, the dominant felsic phase, showing common oscillatory and patchy zoning, the latter suggesting prevalent magma mixing. Glomerocrysts of varied and non-equilibrium phenocryst clusters include several mafic phases, some also containing plagioclase rich in melt inclusions, dominate many deposits. From them we infer advanced crystallization and mixing in magma reservoirs probably distinctly smaller than those beneath Nemrut. These petrographic characteristics, also noted by Özdemir et al. (2011), have been very helpful in distinguishing Süphan tephras from Nemrut ones, which are mostly much less phyric and characterized by largely equilibrium mineral assemblages. Glass shards, commonly only moderately vesicular (<ca. 20 vol.%) in many Süphan tephras contain more or less equant feldspar microlites, also reflecting more-complex eruptive triggering and fragmentation mechanisms. Süphan tephras thus commonly reflect advanced degrees of crystallization, presumably due to complex magma chamber/magma pathway

Table 6 Major compositional contrasts between Nemrut and Süphan tephras

	Nemrut	Süphan
Glass:	(Per-) alkaline	Subalkaline (calcalkaline)
Whole rock trace elements:	LREE + HFS high	LREE + HFS low, Ba + Sr high
Phenocrysts:	Anorthoclase, quartz, fayalite, hedenbergitic cpx, augite	Pl (zoned), alkali feldspar, quartz, cpx, hypersthene, biotite, amphibole, olivine
Equilibrium:	Yes	No
Ascent velocity:	Fast	Slow (microlites)
Types of major deposits:	Fallout, ignimbrite	Fallout and (older) ignimbrite, debris avalanche derived from domes and lava
Tephra coverage of Lake Van:	Complete	Mostly eastern part

structures as well as highly viscous magmas with high silica and an abundance of phenocrysts. In other words, the volcano appears to have grown preferentially from within by sub-volcanic intrusions and domes, a behavior also reflected in large-volume debris avalanche deposits interpreted as due to common flank oversteepening by sub-volcanic intrusions. We speculate that the dominance of turbidites in the sediments drilled at Site 1 (Litt et al. 2011) may be related to the dynamic behavior of Süphan Volcano.

A gradual north–south increase in lava alkalinity has been noted (Nemrut and the older Muş volcanics) (Pearce et al. 1990). A north-to south change from H_2O-rich to H_2O-poor magmas, as expressed by hydrous mineral phases (amphibole, biotite) has also been assumed (e.g., Pearce et al. 1990). This, however, is contradicted by our data because many highly evolved Süphan tephras studied by us are characterized by biotite and some also by amphibole while we have found no biotite or amphibole in any of the ca. 45 Nemrut tephra deposits studied by us.

Discussion

The detailed stratigraphy here documented allows initial and semi-quantitative reconstruction of the *explosive* evolution of the most active volcano of Turkey through at least 400,000 years with respect to

- Temporal history;
- Eruptive and transport mechanisms and dominant hazards;
- Compositional development (magma sources and low pressure differentiation);
- Dependance of the eruptive record on alternating glacial and interglacial stages, including reconstruction of paleowind directions over more than half a million years;
- Geodynamic evolution of the highly active Van Basin, situated in the collision zone between the Arabian and Eurasian plates;
- Evolution of huge Lake Van especially its change from fresh water into a highly alkaline closed lake and the impact of tephra input throughout its evolution.

Temporal evolution of eruptive and transport mechanisms of Nemrut Volcano

As discussed in more detail elsewhere (Sumita and Schmincke 2013a), fallout and pyroclastic flow eruptions in Nemrut Volcano alternated throughout the past 400,000 years at intervals lasting thousands to tens of thousands of years. Most single crystal ages are compatible with their stratigraphic position. As would be expected, the abundance of deposits formed between ca 400 ka and 300–250 ka is lower, most likely due to erosion. Similarly, ignimbrites appear to be more common relative to fallout deposits deposited prior to 200 ka, possibly due to their greater resistance to erosion. Despite these trends, which may reflect climate impacts more than volcano dynamics, the number and frequency of large-volume, mostly rhyolitic fall deposits appears to have increased to prominence since about 300 ka, increasing again with the "mega-tephra" unit AP-1 at ca. 190 ka. The assessment of temporal evolution of tephra frequency given here differs slightly from that proposed in Sumita and Schmincke (2013a, b). The increase in tephra output, reflecting an increase in mass input of parent magma into the substructure of Nemrut Volcano, remained high until the present. Powerful support for this conclusion is provided by a similar increase in Nemrut tephras over roughly the same time interval in the cores drilled during the PaleoVan drilling project (unpublished data) because erosional effects on land should be minimal in the lake sediment "library". Stratigraphic and single crystal age data available are not precise enough to calculate magma output rates per unit time quantitatively for the past ca. 200 ky but data at hand do not indicate major changes. In other words, Nemrut Volcano appears to be alive and well.

Differentiation and compositional evolution

The chemical and mineralogical composition of the trachytes and rhyolites very much resemble those of many other peralkaline systems, crystal fractionation being generally invoked for the derivation of the highly evolved rhyolitic magmas (Pantelleria: Mahood and Hildreth 1986; Gran Canaria: Schmincke and Sumita 1998; large intracontinental rift zones such as the East African Rift: Macdonald and Scaillet 2006; the Baitoushan Volcano (continental rift setting North Korea/China) is the closest analogue: Horn and Schmincke 2000). This line of differentiation has also been inferred by Pearce et al. (1990) and Çubukçu et al. (2012) for Nemrut. Moderately evolved, slightly alkaline to transitional basalts such as those few exposed at Nemrut are the likely parent magma.

The volcanological and stratigraphic data here presented add another perspective to this general model of magmatic evolution. Several land sections (e.g., Fig. 3, 25 km NE of Nemrut and 1–3 km W of Ahlat represented by about 12 fall units separated from each other by moderate paleosols and erosional unconformities; see also Fig. 2) show a general evolution in composition from chiefly high-Si trachytic in the older tephra deposits below the major AP-1 fallout sheet to highly evolved rhyolitic units AP-1 and AP-2 that in turn are overlain by highly peralkaline HP-1 and AP-4 (Fig. 11; Table 1). Dominantly low-Si trachytes were erupted between ca. 82 and 30 ka, before emplacement of NF. We thus tentatively recognize at least four compositional "cycles" developing from trachyte to high silica rhyolite, indicating that extremely fractionated rhyolitic magmas evolved repeatedly in the Nemrut magma reservoirs at several different times (as reflected in the pyroclastic cover): between 160 and 190 ka, at around 130 ka, 60–80 ka and at ca. 30 ka, and in the Holocene although this very young eruption was of minute volume compared to the older ones (see also Fig. 10 in Sumita and Schmincke (2013b)).

New vintages of magma, each with its own distinct trace element signature, were supplied from time to time following large-volume eruptions, i.e. during the intervals between paroxysmal eruptions. Some strikingly distinct compositional groups are especially evident from trace-element abundances. For example, a group of distinct fallout tephra deposits below the NF (Şentepe Formation) are basically low silica trachytes (SiO_2 mostly 63–64 wt.%) with unusually high total alkalis and such high concentrations of several LIL elements such as Zr (1500–1650 ppm) and Nb (97–107 ppm) and LREE that they exceed the concentrations of these elements in the comenditic to pantelleritic rhyolites.

The rhyolitic L-NF fallout initiating the compositionally strongly zoned NF represents the youngest *major* peralkaline rhyolite fall deposits (Fig. 8). NF is separated from the rhyolitic, dominantly phreatomagmatic Holocene tephra spectacularly exposed at the caldera rim of Nemrut (Fig. 12) by ca. 6 to

Fig. 12 Holocene hydroclastic rhyolitic surge, ballistic and fallout deposits mantling the southeastern rim of Nemrut Caldera (loc. 102)

8 mainly high-Si trachytic fall units (Çekmece Formation; Fig. 9d in Sumita and Schmincke (2013a)) that show the highest Ba and Sr concentrations of all samples analyzed, and which also more strongly resemble Süphan tephras than those erupted from Nemrut. Removal of the huge magma volume represented by the NF fall deposits and ignimbrite together, probably $\gg 10$ km^3 DRE, during a single eruption must have upset the stress field between the marginally overlapping Nemrut and Süphan systems, and may have facilitated temporary magma transfer from the Süphan to the Nemrut reservoir. "Normal" Nemrut compositions were restored by the time late Holocene (?) rhyolitic phreatomagmatic deposits were emplaced at the caldera margin.

Volcanism in the framework of the geodynamic evolution of the highly active Van basin in the active collision zone between the Arabian and Eurasian plates

Although the focus of our work is on tephra deposits, there is much evidence that volcanism in a still highly active collision zone was profoundly influenced by tectonism. For example, Nemrut Volcano grew in the hinge zone between two tectonic pull-apart basins: the east–west-oriented Van Basin to the east and the extremely flat-floored Muş Basin extending for ca. 50 km west-southwest of Nemrut Volcano. It is logical to infer that the position of Nemrut in a location between the two basins is not fortuitous. Syn- and post-volcanic faults throughout the area studied by us are ubiquitous. We noted two major fault orientations: north–south, possibly deeper-reaching ones, that allowed basaltic magmas to reach the surface, and subsidiary southwest-northeast-oriented ones. The impressive Halepkalesi deformation belt whose uplift and deformation history has a direct bearing on the products of explosive volcanism and timing and origin of the alkaline Lake Van system has been

briefly described by Sumita and Schmincke (2013a). Regional deformation will be discussed in more detail elsewhere (Schmincke et al. in prep.).

Paleoclimate evolution over more than half a million years

Because the main aim of the ICDP PaleoVan project that provides the overall framework for this study is paleoclimate reconstruction, we will briefly discuss some paleoclimate proxies and indirect types of evidence that demonstrate that the role of volcanism has, in the past, not received due attention in reconstructing the evolution of the Lake Van System.

1. *Environmental proxies and impacts of pyroclastic eruptions*

The environmental impacts—and resulting proxies—of a succession of many major pyroclastic eruptions over >400,000 years on the land surface around huge Lake Van and its sediment and water fill at a time of dominantly dry climate have been manifold and massive. North and northwest of the lake, basically the Ahlat hinterland, we found no widespread epiclastic sediments, but only primary fallout and flow deposits interbedded with reworked volcaniclastic Intra-Tephra Deposits (ITD, see above). Most ITDs are presumably dominantly variably wind-reworked tephras including remnants of primary tephra layers except in the river canyon that drains the lower Süphan slopes and inside the town of Ahlat. Here, well-bedded coarse volcaniclastic (near-shore?) sediments >10 m thick that also contain limestone fragments and are eroded at the top unconformably overlie AP-1 and AP-2 fallout at ca. 1,770 m asl (loc. 31). These sediments could have been laid down during a period of lake high stand sometime after 160 ka, the age of the youngest tephra unit preserved in situ (AP-2), but could also be quite young. In view of the pronounced syn- and post-volcanic deformation in this general area (e.g., a major, roughly N–S oriented morphologically expressed graben with >10 m of displacement is crossed by the main road Ahlat–Lake Nazik) we are reluctant, however, to infer ancient lake high stands from this outcrop.

Incomplete development of clay-rich paleosols between tephra units, the general absence of vegetation (for an exception see Fig. 13) and dominant wind erosion and reworking of unconsolidated tephra suggests dry conditions prevailing through much of at least the past ca. 400 ky, reflecting a sensitive environment highly susceptible to external forcing such as massive *pyroclastic sealing*. In other words, soil development, however subtle, has been repeatedly interrupted by tephra falls and/or ignimbrites that seal the pre-eruption surface from further surface weathering. At present, there is a striking contrast between the dry, steppe-like environment of the lowlands and that of the more subdued mountains. The former are the arid eastern and northern slopes of Nemrut edifice, west and east of Ahlat, north and northwest of western Lake Van, while the latter are the more humid and thus vegetated high mountains and steep valleys of the mountainous Bitlis massif that rises to more than 3,000 m asl bordering Lake Van to the south. Consequently, more mature paleosols between tephra deposits are slightly more common between tephra deposits south of Lake Van suggesting that the present regional climatic contrasts have persisted since at least 500 ka. Moreover, conglomerates several m thick interbedded with tephra deposits reflect severe and rapid erosion, and occur locally south of Lake Van. The south-southeast-facing slopes of the Nemrut edifice and uplifted shoulders of the Muş Graben system that are exposed

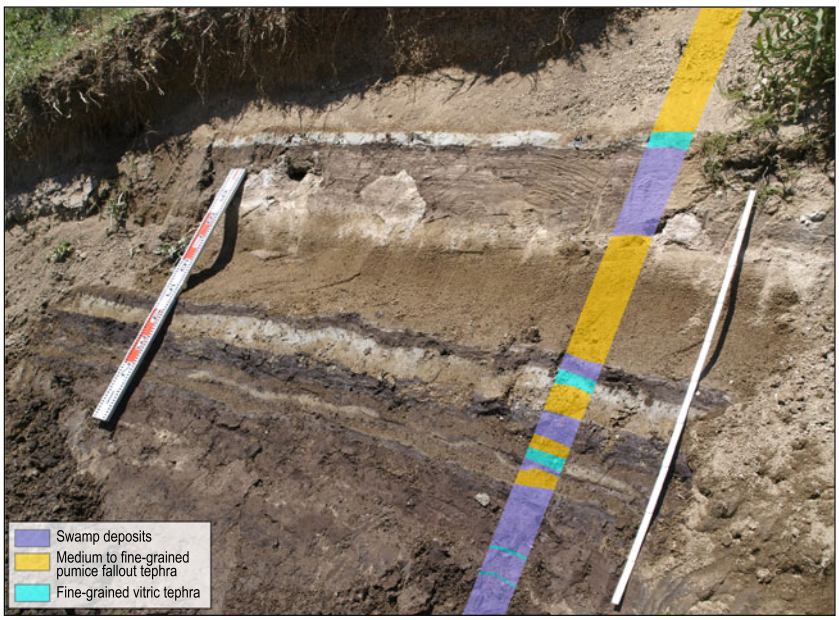

Fig. 13 Several thin (*lower part of photograph*) and thicker tephra layers (*upper part of photograph*) (Derin River Formation, ca. 80 ka old) interlayered with dark swamp deposits ca. 20 km east of Tatvan (loc. 145; see also Fig. 2, section E-1). These wet climate conditions are also documented by abundant root and tree molds in the overlying basaltic İncekaya tephra deposits

to the dominant south-southwest directed wind system show more intense weathering. This effect must have become progressively more pronounced as Nemrut edifice and its outlying domes grew in elevation with time.

Present wind directions are WSW to WNW. From the ca. 14 larger fall tephra fans correlated over the area and with thicknesses and grain size measured at three or more localities, dominant wind directions are inferred to have been fairly stable since 400 ka, practically identical to present day directions. The axes of the fallout fans of the two youngest major fallout fans from Nemrut—HP-10/AP-6 (ca. 60 ka) and L-NF (ca. 30 ka)—are oriented west–east reflecting westerly (Fig. 5b), contrasted with dominant SW wind directions for the older tephra layers. Whether or not this reflects a change in dominant wind direction or not is uncertain. In any case, the tight tephra fan of L-NF suggests high wind velocities and a constant direction during the eruption.

2. *Rapid rise and lowering of lake level*: *climate forcing* (*alternating periods of massive precipitation and subsequent droughts*) *or volcanic*/*geodynamic forcing*, *or both*? *A precisely dated case history reflects significant climatic forcing along southeastern Halepkalesi peninsula*: *the remarkable drowning and resurfacing of the L-NF pumice fallout deposit at Halepkalesi beach* (Fig. 14).

The base of well-dated ca. 30 ka rhyolitic L-NF (Fig. 14b, c) overlies at lake level an ITD below which the top of HP-10 (ca. 60 ka), well-exposed farther west, is barely visible under water. Most of the NF deposits are removed by shallow water erosion, and we correlate the 2 m-thick erosional remnant to the more fully preserved L-NF in an abandoned pumice pit ca. 2.5 km to the west where L-NF is ca. 13 m thick (Fig. 14c; loc. 72 in Fig. 7). At the beach section, L-NF is overlain by ca. 10 m of pebbly to sandy-bedded shallow water volcaniclastic sediments no doubt largely derived by erosion mainly from L-NF. Farther east along the cliff, L-NF is completely eroded. The reworked deposits are topped by a weakly developed soil. Structural evidence shows unequivocally that L-NF now exposed on land was also deposited subaerially—as were the underlying fall deposits outcropping along cliffs farther to the west. This sequence of fallout deposits must, therefore, have (a) been deposited subaerially, (b) been subsequently inundated and eroded subaqueously and (c) returned back to subaerial conditions. Which parts of the system have moved, the land or the lake level or both—and when and how fast and why?

A rise in lake level not only would have affected remnant NF and overlying clastic sediments—combined total thickness ca. 10 m—but also possibly 20 m or more which includes the underlying HP-10 and other subaerially deposited fallout tephras overlying the uplifted Halepkalesi cliff section described above and dated as 160 ka and younger (Fig. 2, section H; Fig. 5 in Sumita and Schmincke (2013a)). The level of Lake Van must have been significantly lower than at present because there is no evidence that underlying HP-10 was not deposited on land—or the land surface significantly higher. Given the thickness of HP-10 (ca. 12 m in this area), its upper surface when deposited lay at least 15 m above lake level, possibly significantly more. Moreover, the agglutinate member of NF dips steeply into Lake Van at several places between Halepkalesi and Tatvan, further evidence that both HP-10 and upper members of NF were deposited well above lake level at ca. 30 ka and before. In other words, lake level must have been significantly lower than today prior to ca. 30 ka. Seismic evidence acquired in August 2012 confirms the long-held suggestion of significantly lower lake level prior to ca. 15 ka (Cukur pers. comm.)—but after L-NF (30 ka). We here suggest that the level of Lake Van at 30 ka was (a) much lower than at present, (b) quickly rose soon after emplacement of NF, (c) subsequently fell by some 240 meters before it (d) finally (probably between ca. 15 ka and today) rose to its present level.

Several mechanisms can theoretically explain a significant and very rapid rise and fall of lake level following emplacement of NF—and underlying tephra deposits—subaerially: (a) Vertical subsidence of the eastern lower flanks of Nemrut volcanic edifice—or parts thereof—following eruption of NF—by several meters soon after eruption is possible and would explain the massive elevation changes; we have documented uplift of tens if not hundreds of m in western Halepkalesi Peninsula (see above). The main Nemrut magma reservoir was drastically exhausted following the NF eruption, and modest eruptive and thus possibly magma recharge rates meant it was not "refilled" for some time. Trace element patterns for post-NF tephras on land show Süphan-type characteristics, suggesting that collapse of the Nemrut system may have allowed influx of Süphan-type magmas into the Nemrut system. Inter-volcano lateral magma transfer of 10 km is well known from historic eruptions, as well documented at Katmai (Hildreth and Fierstein 2012). (b) A total thickness of 15 m of NF tephra (fallout plus turbidites transformed from ignimbrite entry into the lake) was deposited on the lake floor based on recent seismic (Cukur pers. comm.) and drilling evidence (unpublished). Unknown volumes of tephra were also washed down from the flanks of the enclosing mountains soon after the eruption, adding perhaps several m of solid material to the floor of the lake thereby raising lake level quickly. (c) Since the ca. 30 ka transgression probably started from a very low preceding lake level (our data), we suggest that massive loading of the eastern—now sublake—lower flanks of Nemrut by major lake level increase may have triggered the NF eruption. The effect of lithospheric loading on earthquakes, even by minor Van lake level

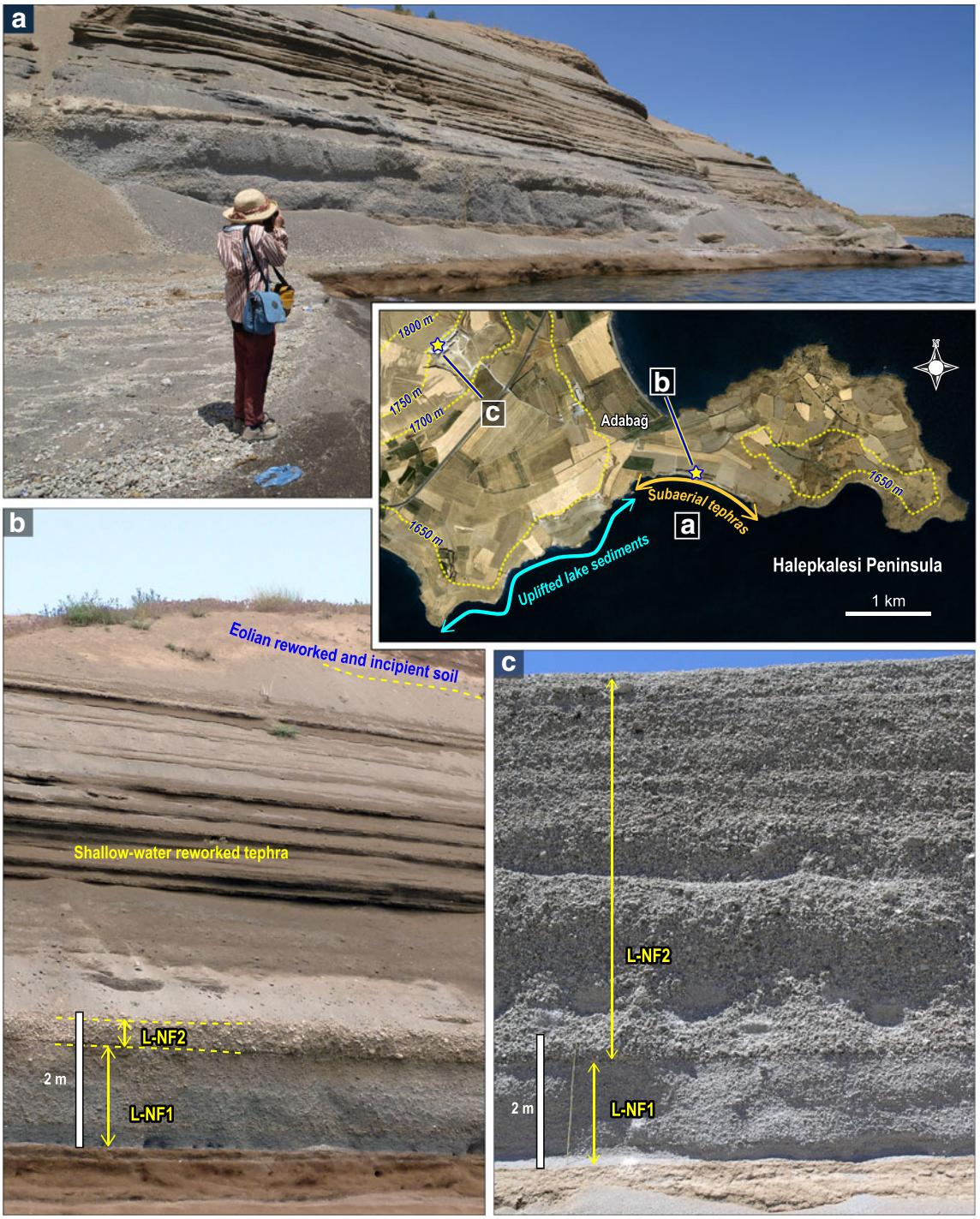

Fig. 14 Photographs of eastern end of Halepkalesi Peninsula east of deformation belt along coast of western Lake Van. **a** Overview (loc. 74). **b** Subaerially deposited L-NF (loc. 74), almost completely eroded, is overlain by bedded shallow water reworked tephra. Note present lake level ca. 1,640 m asl. **c** Thick (12 m) L-NF fallout tephra at Adabağ pumice pit (loc. 72, 1,750 m asl)

changes has recently been demonstrated, with temporal correlations of seismicity with the water level changes being "very persuasive and dramatic, indicating hydrogeological triggering of the earthquakes" (Utkucu 2006). (d) Strongly humid conditions (massive precipitation) are well known to have prevailed in the eastern Mediterranean at this time (at ca. 30 ka) and have been invoked by Kuzucuoğlu et al. (2010) to explain terraces, up to 20 m above lake Van's present shoreline level. An early lake-level lowstand followed by inundation would fit the evidence from the Halepkalesi section well. Moreover, invoking a rise of lake level from a much lower level expands the model for lake-

level variation, adding to the ca. four times lake level low stands invoked previously (see above). A climate-controlled rise in lake level could, of course, be enhanced by deposition of the voluminous L-NF tephra sheet on the lake bottom, which would help explain the rapid pace of lake level rise. Incessant rain would also contribute to quick removal of tephra from the mountain slopes. In short, climate-controlled fast rise and fall of the level of Lake Van could explain subaerial tephra deposition followed by drowning at eastern Halepkalesi peninsula especially in view of the impressive temporal coincidence of the age of L-NF eruption and of the humidity peak. A significant subsequent drop in lake level—as reflected in the soil topping the epiclastic sediments overlying L-NF—also coincides with a major drop in lake levels in the eastern Mediterranean at ca. 20 ka as postulated by many workers (see Kuzucuoğlu et al. (2010) for discussion). However, whether or not climate forcing alone (i.e. evaporation, cloud changes and reduced orographic rainfall) can account for a major drop of the level of a huge lake in some 15,000 years needs to be well documented; a more in-depth analysis of differential lithosphere reaction to high but variable loads in the Van basin is highly desirable.

In summary, the Halepkalesi beach section is clearly a key location for more quantitatively assessing rates of lake level rise and fall modulated by climate and possibly modulated or enhanced by volcanic forcing mechanisms and differential lithospheric loading.

Hazards

The Lake Van area is developing at a rapid pace. The lake is encircled by excellent modern highways and the major towns Van, Tatvan, Erciş and Ahlat are growing at a fast pace as witnessed by ongoing construction activities. Relevant volcanic hazards derived from the new stratigraphy here presented include: Large-magnitude mostly rhyolitic explosive eruptions, several with volumes (DRE) > 5 km^3, occur at intervals of 20–40,000 years and several produced pyroclastic flows. Based on past eruption styles and general periodicity alone, the next major Plinian eruption could take place at any time, since the Nemrut eruption (NF) occurred 30,000 years ago. Such an eruption would represent a high-risk event especially for the western Lake Van area between the towns of Tatvan and Ahlat. Our work shows that pyroclastic flows, the major hazard on land, have occurred repeatedly throughout the history of Nemrut Volcano and many immediately succeeded major fallout phases of an eruption, as for example NF. Powerful tsunamis are likely to be generated when large pyroclastic flows enter the lake as demonstrated recently for Lake Managua (Freundt et al. 2007). Such tsunamis could be a major risk also for the distant towns at the northern and eastern shores of Lake Van: Adilcevaz, Van, and Erciş. Several debris avalanche deposits of young age (possibly late Holocene) recognized by us near the northern outskirts of Tatvan and along the north shore are another major hazard, especially since they are also tsunamogenic when debouching into Lake Van. The major and more frequent natural hazards in the area are, of course, large earthquakes, the most recent one having occurred on October 23, 2011 in the vicinity of the city of Van resulting in more than 600 deaths and destruction of >2,000 houses. A temporal and causal relationship between large earthquakes and ensuing volcanic eruptions has been recognized over the past decades globally and should be applicable to the Van Basin as well. We thus speculate that the probability of an explosive eruption in the near future has increased following the devastating magnitude 7 earthquake on October 24, 2011. Another major hazard are debris avalanches from Nemrut or Süphan that could be catastrophic for the towns at the feet of the lower slopes of the volcanoes: Tatvan, Ahlat, and Adilcevaz. Eruptions of Nemrut Volcano may be triggered preferentially by magmatic forcing while we tentatively interpret the cluster of (small) Süphan eruptions of late-glacial age (Sumita and Schmincke 2009) as externally triggered, possibly by preceding long lasting earthquake activity and/or fluctuating stress conditions in the lithosphere resulting from major lake level changes (e.g., Utkucu 2006) or melting of large volumes of ice.

Conclusions

1. We document the first detailed regional tephrostratigraphic framework of Nemrut Volcano. Approximately 45 major trachytic to rhyolitic Plinian fallout deposits (DRE volumes up to ≫10 km^3) and ca. 12 major trachytic to rhyolitic ignimbrites, both plateau-forming and valley-confined, sourced in active Nemrut Volcano beginning before 400 ka have been stratigraphically correlated over >6,000 km^2, dated and compositionally characterized. The oldest dated of ca. 12 ignimbrite sheets found covers the highland southwest of Nemrut and formed at ca. 250 ka; the multiple sheets indicate several caldera collapse stages of Nemrut Volcano.
2. Süphan volcanic deposits differ mineralogically and chemically from those of Nemrut and reflect derivation of its magma from a subduction-zone related source. Süphan magmas are interpreted to reside in relatively small reservoirs and generally tend to form domes and sub-volcanic intrusions rather than voluminous tephra deposits.
3. Isolation of Lake Van is tentatively suggested to have resulted from the growth of Nemrut edifice prior to 400 ka—probably before 500 ka—in the hinge area between the Muş and Van pull-apart graben structures.
4. The lake had become alkaline certainly by 200 ka and possibly before 400 ka—based on the age of uplifted

tephra beds interbedded with carbonate lake sediments. Massive influx of highly alkaline fine-grained tephra into the lake, alkaline groundwater from beneath the volcanoes and possibly intralake hydrothermal springs may have contributed to the alkaline composition of Lake Van as much as has climate.

5. Nemrut explosive products since 400 ka or before are characterized by equilibrium phenocryst assemblages and peralkaline compositions that indicate low viscosity magmas. The episodicity of large-volume mostly rhyolitic explosive eruptions at 20–40 ky intervals, separated by smaller trachytic eruptions, may indicate a dominant mode of relatively constant magma supply from depth. Periods when small volumes of magma underwent moderately high levels of differentiation have been punctuated by episodic large-volume eruptions of highly evolved magma that accumulated to a critical threshold volume. Similar incompatible trace-element signatures of groups of trachyte tephras erupted between large-volume rhyolite eruptions changed drastically following the next major—rhyolitic—eruption suggesting repeated significant resetting of the magmatic system.
6. A significantly lower lake level prior to 30 ka and possibly as early as 120 ka, is well supported. A rapid rise of lake level soon after deposition of L-NF (ca. 30 ka), reflected in the almost complete erosion of L-NF deposits decreasing landwards, could be attributed to heavy precipitation as found throughout much of the Eastern Mediterranean at this time, and possibly aided by deflation of Nemrut edifice following discharge of magma to form the voluminous NF deposits. To what degree the subsequent lowering in lake level was entirely climate-controlled or also by rise of the ground at the west end of the lake due to magmatic swelling is unknown.

Acknowledgments The goal of our work was the need for a pre-site survey of the widespread but poorly known explosive products of Nemrut and Süphan volcanoes related to, and accompanying, the ICDP PaleoVan drilling project (Litt et al. 2011) because of the expected major stratigraphic, temporal and compositional contribution of tephra layers to the Lake Van sediments. Our work was financed by DFG projects SCHM 250/86-1 and 87–1. We thank Mario Thöner for help with the microprobe and Dieter Garbe-Schönberg for support with the HF-cleaning of anorthoclase crystals for single crystal dating. We thank Ray Macdonald for helpful comments on the text. The manuscript was much improved by reviewer Emma Tomlinson and James White who went over the entire manuscript with a fine pen.

Appendix

Bulk XRF analyses

Selected rock fragments (pumice lapilli) were crushed in a jaw crusher, pulverized in agate mills and dried at 110 °C in an oven for about 12 h to drive off moisture. Fused beads were prepared by mixing 600 mg sample powder with 3,600 mg lithium tetraborate ($Li_2B_4O_7$). The mixture was melted at about 1,000 °C; the melt was cast into a preheated mold and slowly cooled to avoid shattering due to thermal stress. Major elements and selected trace elements were determined on a fully automated WDS X-ray fluorescence spectrometer equipped with a Rh-tube (Panalytical Magix Pro). International rock standards prepared as described above were used for internal calibration according to the recommended values given by Govindaraju (1994). Several international standards were run as unknowns and the measured values are in good agreement with the recommended values. Detection limits for major elements are <0.01 wt% except for Na_2O and MgO, which are <0.02 wt%. Detection limits for trace elements are generally lower than 10 ppm except for Ba, La, Ce, and Nd which are ca. 20 ppm. LOI (loss-on ignition) was determined gravimetrically at 1,050 °C for 1 h (Lechler and Desilets 1987).

EMP analyses

Major elements and S, Cl, and F of glassy groundmasses and minerals of tephra particles were carried out with a JEOL JXA 8200 electron microprobe (EMP) at the GEOMAR Helmholtz Institute for Ocean Research Kiel. Analytical conditions were 15 kV of accelerating voltage, 6 nA of beam current for felsic glass, 10 nA for sideromelane, feldspar, amphibole, and mica, 20 nA for pyroxene, and 20 s of peak counting time. Analyses were performed with an electron beam rastered to 5×5 μm in the scanning mode for felsic glass, sideromelane, feldspar, and 10×10 μm for other minerals. Basaltic glasses USNM 111240/52 and USNM 113498/1 (VG-A99), apatite USNM 104021, and microcline USNM 143966 (Jarosewich et al. 1980) were used as standards for calibration.

Analyses of phenocrysts of feldspar, pyroxenes, olivine and glass shard were selected from either grain mount polished sections of sieved tephra samples (generally −1 to −2 phi) or polished sections of solid rock (or pumice) samples. As shown in Tables 2, 3, 4 and 5, several points were analyzed in single grains (number of analyses) and recalculated as average. We here only show analyses of the cores of phenocrysts.

References

Aydar E, Gourgaud A, Ulusoy İ, Digonnet F, Labazuy P, Şen E, Bayan H, Kurttas T, Tolluoğlu AÜ (2003) Morphological analysis of active Mount Nemrut stratovolcano, eastern Turkey: evidences and possible impact of future eruption. J Volcanol Geotherm Res 123:301–312

Çubukçu HE, Aydar E, Gourgaud A (2007) Comment on "Volcanostratigraphy and petrogenesis of the Nemrut stratovolcano

(East Anatolian High Plateau): The most recent post-collisional volcanism in Turkey" by Özdemir et al. [Chemical Geology 226 (2006) 189–211]. Chem Geol 245: 120–129

Çubukçu HE, Ulusoy İ, Aydar E, Ersoy O, Şen E, Gourgaud A, Guillou H (2012) Mt. Nemrut volcano (Eastern Turkey): Temporal petrological evolution. J Volcanol Geotherm Res 209–210:33–60

Cukur D, Krastel S, Demirel-Schlüter F, Demirbag E, Imren C, Niessen F, Toker M, Paleo Van-Working Group (2012) Sedimentary evolution of Lake Van (Eastern Turkey) reconstructed from high resolution seismic investigations. Int J Earth Sci 102:571–585. doi:10.1007/s00531-012-0816-x

Dewey JF, Hempton MR, Kidd WSF, Şaroğlu F, Şengör AMC (1986) Shortening of continental lithosphere: the neotectonics of Eastern Anatolia—a young collision zone. In Collision Tectonics, Coward Mp, Ries AC (eds). Geol Soc Spec Publ 19:3–36

Degens ET, Kurtmann F (1978) The geology of Lake Van. MTA Press, Ankara, pp 1–158

Fisher RV, Schmincke H-U (1984) Pyroclastic rocks. Springer, Berlin, pp 1–472

Freundt A, Schmincke H-U, Kutterolf S (2007) Volcanogenic tsunamis in lakes: examples from Nicaragua and general implications. Pure Appl Geophys (PAGEOPH) 164:527–545

Govindaraju K (1994) 1994 compilation of working values and sample description for 383 geostandards. Geostand Newslett 18:1–158. doi:10.1046/j.1365-2494.1998.53202081.x-i1

Haroutiunian RA (2006) The historical volcanoes of Armenia and adjacent areas revisited. J Volcanol Geotherm Res 155:334–337

Hildreth W, Fierstein J (2012) The Novarupta-Katmai eruption of 1912—largest eruption of the twentieth century: centennial perspectives. US Geol Surv Prof Paper 1791: 259 p

Horason G, Boztepe-Güney A (2007) Observation and analysis of low-frequency crustal earthquakes in Lake Van and its vicinity, eastern Turkey. J Seism 11:1–13

Horn S, Schmincke H-U (2000) Volatile emission during the eruption of Baitoushan Volcano (China/North Korea) ca. 969 AD. Bull Volcanol 61:537–555

Jarosewich E, Nelen JA, Norberg JA (1980) Reference samples for electron microprobe analysis. Geostand Newsl 4:43–47

Karakhanian A, Djrbashian R, Trifonov V, Philip H, Arakelian S, Avagian S (2002) Holocene-historical volcanism and active faults as natural risk factors for Armenia and adjacent countries. J Volcanol Geotherm Res 113:319–344

Karaoğlu Ö, Özdemir Y, Ümit Tolluoğlu A, Karabiyikoğlu M, Köse O, Froger J-L (2005) Stratigraphy of the volcanic products around Nemrut Caldera: Implications for reconstruction of the caldera formation. Turkish J Earth Sci 14:123–143

Keskin M (2003) Magma generation by slab steepening and break off beneath a subduction-accretion complex: An alternative model for collision-related volcanism in Eastern Anatolia, Turkey. Geophys Res Lett 30:8046. doi:10.1029/2003GL018019

Keskin M (2007) Eastern Anatolia: a hotspot in a collision zone without a mantle plume. Geol Soc Am Spec Pap 409:475–505

Kuzucuoğlu C, Christol A, Mouralis D, Doğu A-F, Akköprü E, Fort M, Brunstein D, Zorer H, Fontugne M, Karabiyikoğlu M, Scaillet S, Reyss J-L, Guillou H (2010) Formation of the Upper Pleistocene terraces of Lake Van (Turkey). J Quat Sci 25:1124–1137

Landmann G, Reimer A, Lemcke G, Kempe S (1996) Dating late glacial abrupt climate changes in the 14,570 years long continuous varve record of Lake Van, Turkey. Palaeogeogr Palaeoclimatol Palaeoecol 122:107–118

Le Bas MJ, LeMaitre RW, Streckeisen A, Zanettin B (1986) A chemical classification of volcanic rocks based on the total alkali-silica diagram. J Petrol 27:745–750

Lechler PJ, Desilets MO (1987) A review of the use of loss on ignition as a measurement of total volatiles in whole rock analyses. Chem Geol 63:341–344

Litt T, Krastel S, Sturm M, Kipfer R, Örcen S, Heumann G, Franz SO, Ülgen BU, Niessen F (2009) PALEOVAN, Intern Cont Sci Drill Prog (ICDP): Site survey results and perspectives. Quat Sci Rev 28:1555–1567

Litt T, Anselmetti FS, Cagatay N, Kipfer R, Krastel S, Schmincke H-U, PaleoVan scientific team (2011) A 500,000 year-long sedimentary archive drilled in Eastern Anatolia (Turkey): The PaleoVan Drilling Project. Eos 92:477–479

Litt T, Anselmetti FS, Baumgarten H, Beer J, Çağatay N, Cukur D, Damci E, Glombitza C, Haug G, Heumann G, Kallmeyer GJ, Kipfer R, Krastel S, Kwiecien O, Meydan OF, Orcen S, Pickarski N, Randlett M-E, Schmincke H-U, Schubert CJ, Sturm M, Sumita M, Stockhecke M, Tomonaga Y, Vigliotti L, Wonik T, the PALEOVAN Scientific Team (2012) 500,000 years of environmental history in Eastern Anatolia: the PALEOVAN Drilling Project. Scientific Drilling 14: 18–29. doi:10.2204/iodp.sd

Macdonald R (1974) Nomenclature and petrochemistry of the peralkaline oversaturated extrusive rocks. Bull Volcanol 38:498–516

Macdonald R, Scaillet B (2006) The central Kenya peralkaline province: Insights into the evolution of peralkaline salic magmas. Lithos 91:59–73

Mahood GA, Hildreth W (1986) Geology of the peralkaline volcano at Pantelleria, Strait of Sicily. Bull Volcanol 48:143–172

Mouralis D, Kuzucuoğlu C, Akköprü E, Doğu A-F, Scaillet S, Christol A, Zorer H, Brunstein D, Fort M, Guillou H (2010) Les pyroclastites du Sud-Ouest du Lac de Van: implications sur la paleo-hydrographie regionale. Quaternaire 21:417–433

Özdemir Y, Blundy J, Güleç N (2011) The importance of fractional crystallization and magma mixing in controlling chemical differentiation at Süphan stratovolcano, eastern Anatolia, Turkey. Contrib Mineral Petrol 162:573–597

Özdemir Y, Karaoğlu Ö, Ümit Tolluoğlu A, Güleç N (2006) Volcanostratigraphy and petrogenesis of the Nemrut stratovolcano (East Anatolian High Plateau): the most recent post-collisional volcanism in Turkey. Chem Geol 226:189–211

Pearce JA, Bender JF, De Long SE, Kidd WSF, Low PJ, Güner Y, Şaroğlu F, Yılmaz Y, Moorbath S, Mitchell JG (1990) Genesis of collision volcanism in eastern Anatolia, Turkey. J Volcanol Geotherm Res 44:189–229

Schmincke H-U, Sumita M (1998) Volcanic evolution of Gran Canaria reconstructed from apron sediments: Synthesis of VICAP project drilling (ODP Leg 157). In: Weaver PPE, Schmincke H-U, Firth JV, Duffield WA (eds) Proc ODP, Sci Results 157: 443–469

Schmincke H-U, Sumita M (2013) Fire in the sea—Growth and destruction of submarine volcanoes. Geology 41:381–382. doi:10.1130/focus0320132.1

Selcuk L, Selcuk AS, Beyaz T (2010) Probabilistic seismic hazard assessment for Lake Van Basin, Turkey. Nat Hazards 54:949–965

Şengör AMC, Özeren S, Genç T, Zor E (2003) East Anatolian high plateau as a mantle-supported, north–south shortened domal structure. Geophys Res Lett 30:8045. doi:10.1029/2003GL017858

Sumita M, Schmincke H-U (2009) Explosive volcanism during evolution of Lake Van. Abs volume IODP-ICDP Kolloquium 2009 (Potsdam): 161–162

Sumita M, Schmincke H-U (2012) The climatic, volcanic and geodynamic evolution of the Lake Van-Nemrut-Süphan system (Anatolia) over the past ca. 550–600 000 years. A progress report based on a study of the products of explosive volcanism on land and in the lake. Extended abstract. Abs volume IODP-ICDP Kolloquium 2012 (Kiel): 157–162

Sumita M, Schmincke H-U (2013a) Impact of volcanism on the evolution of Lake Van II: Temporal evolution of explosive volcanism

of Nemrut Volcano (eastern Anatolia) during the past ca. 0.4 Ma. J Volcanol Geotherm Res 253:15–34

Sumita M, Schmincke H-U (2013b) Erratum to "Impact of volcanism on the evolution of Lake Van II: Temporal evolution of explosive volcanism of Nemrut Volcano (eastern Anatolia) during the past ca. 0.4 Ma." J Volcanol Geotherm Res 253: 131–133. doi:10.1016/j.jvolgeores.2013.01.008

Taymaz T, Yılmaz Y, Dilek Y (2007) The geodynamics of the Aegean and Anatolia: introduction. *In*: Taymaz T, Yılmaz Y, Dilek Y (eds) The Geodynamics of the Aegean and Anatolia, Geol Soc London, Sp Pub 291: pp 1–16

Ulusoy İ, Çubukçu HE, Aydar E, Labazuy P, Ersoy O, Şen E, Gourgaud A (2012) Volcanological evolution and caldera forming eruptions of Mt. Nemrut (Eastern Turkey). J Volcanol Geotherm Res 245–246:21–39

Ulusoy İ, Labazuy P, Aydar E, Ersoy O, Çubukçu E (2008) Structure of the Nemrut caldera (Eastern Anatolia, Turkey) and associated hydrothermal fluid circulation. J Volcanol Geotherm Res 174: 269–283. doi:10.1016/j.jvolgeores.2008.02.012

Utkucu M (2006) Implications for the water level change triggered moderate (M≥4.0) earthquakes in Lake Van basin, Eastern Turkey. J Seism 10:105–117. doi:10.1007/s10950-005-9002-yC

Yılmaz Y, Güner Y, Şaroğlu F (1998) Geology of the Quaternary volcanic centres of the east Anatolia. J Volcanol Geotherm Res 85:173–210